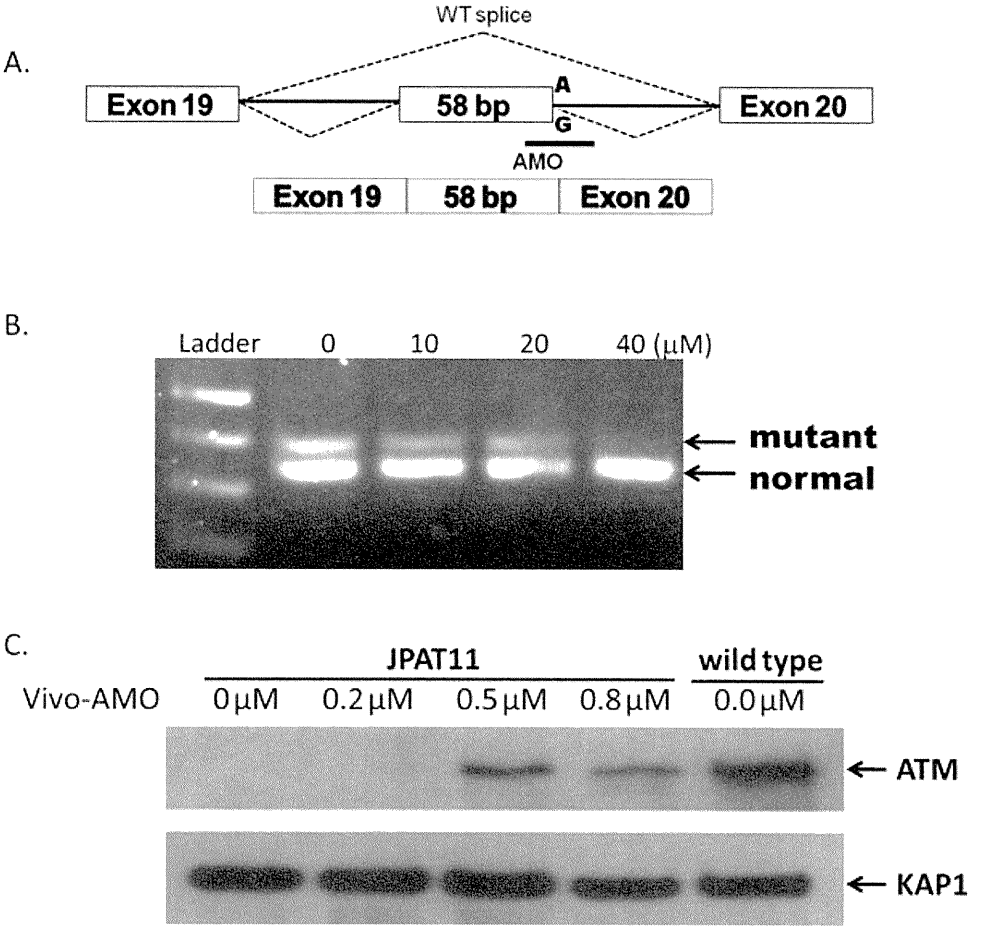

Figure 5. Correction of a splicing mutation in JPAT11 using AMO-J11. **(A)** Schematic representation of inclusion of pseudoexon (type II) and location of designed AMO. **(B)** JPAT11 cells were treated with 0, 10, 20, and 40 μM AMO for 4 days and RNAs were isolated and analyzed for corrected splicing products. **(C)** JPAT11 cells were treated with 0.2, 0.5, and 0.8 μM of Vivo-AMO-J11 for 4 days and nuclear lysates were isolated for western blotting. KAP1 antibody was used as a loading control.

days, and measured ATM autophosphorylation after DNA damage induced by IR. An aminoglycoside RTC, G418, served as a positive control. Both G418 and RTC13 successfully induced ATMpS1981 autophosphorylation as shown by (A) FC-ATMpSer1981 and (B) IRIF ATMpSer1981 assays (Fig. 6), thereby demonstrating a potential therapeutic approach for these siblings, despite the presence of a nonsense mutation in only one allele.

Discussion

Whereas a high (0.5%) coefficient of inbreeding had been recorded for the Japanese population [Pattison, 2004], the *ATM* mutation spectrum identified in our JPAT patient cohort included almost no homozygous mutations and no founder mutations. The c.4776+2T>A and c.7883_7887del5 mutations reported by Ejima and Sasaki [1998] and Fukao et al. [1998] were not observed. In fact, all mutations detected in the JPAT families—four frameshift, two nonsense, four LGDs, and six affecting splicing—were new except for a previously identified c.748C>T splicing mutation in an Irish–American family [Teraoka et al., 1999] and the c.2639-384A>G mutation [Sobeck, 2001]. It is noteworthy that only three of the six splicing mutations involved canonical sites (c.331+5G>A, c.2639-19_2639-7del13, c.8585-1G>C). In the other mutations: (1) c.748C>T (exon 9) and 4956GC>TT (exon 35) presented as nonsense mutations in gDNA, but at the cDNA level caused skipping of the exon in which they were located; and (2) JPAT11/12 had a deep-intronic mutation (c.2639-384A>G) in intron 19 that seemed to activate a cryptic acceptor splice site resulting in the insertion of a 58-bp pseudoexon in the transcript (Figs. 1, 2C, and 5).

Nonsense mutations frequently alter the splicing of the exon containing them, an observation that has been termed nonsense-associated altered splicing (NAS) [Valentine, 1998]. In most cases of NAS, the mutation disrupts an ESE critical for exon inclusion [Liu et al., 2001]. AMOs usually act by covering/masking a mutated site in the pre-mRNA, but cannot be used to correct splicing mutations at canonical sites. Thus, AMOs are most effective in correcting type II and IV splice mutations [Eng et al., 2004]. Most relevant here, AMOs can be applied to the functional analysis of *ATM* mutations. By using AMOs designed to bind the wild-type exon 9 and exon 35 sequences located around the mutation sites, we were able to induce alternative splicing (Fig. 2G and H). These results suggest that unknown regulatory elements are probably located near or at the sites of the mutation and are necessary for modulating normal splicing events in these exons. Furthermore, as described earlier, the deep-intronic mutation (c.2639-384A>G) in intron 19 is among the most attractive candidates for AMO therapy (Fig. 5) [Du et al., 2007].

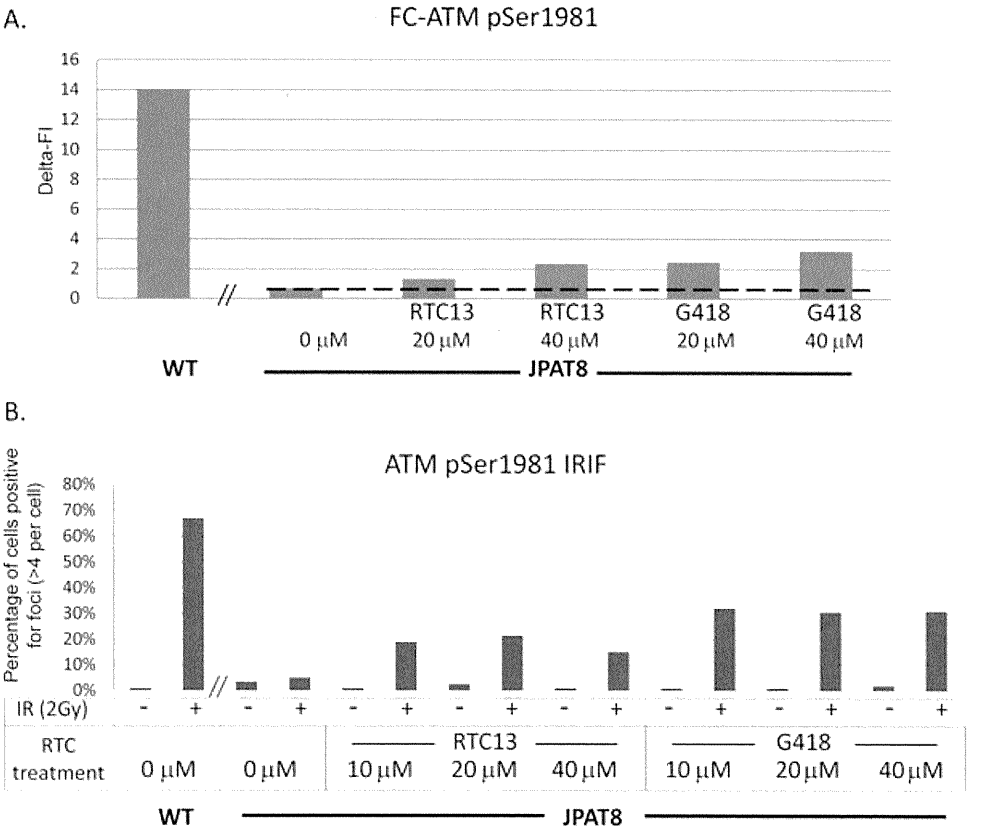

Figure 6. Readthrough compounds (RTCs) restored ATMpSer1981 autophosphorylation in JPAT8 LCL with a nonsense mutation. Cells were treated with readthrough compounds RTC13 and G418 for 4 days and then analyzed for ATMpSer1981. **(A)** ATMpSer1981 autophosphorylation level measured by FC-ATMpSer1981. Delta FI (fluorescence intensity) reflects the difference in FI between nonirradiated and irradiated cells. The data represent one of three independent experiments and results were consistent. **(B)** ATMpSer1981 foci formation by IRIF assay. The data are an average of two independent experiments.

LGDs and duplications within the *ATM* gene account for approximately 2% of reported mutations [Cavalieri et al., 2006, 2008; Coutinho, et al., 2004; Ejima and Sasaki, 1998; Gilad et al., 1996b; Mitui et al., 2003; Telatar et al., 1998b]. Few LGDs have been found in a homozygous state in A-T patients [Mitui et al., 2003]. The recent introduction of the MLPA technique has greatly improved the detection of genomic rearrangement mutations, including LGD and duplications in the *ATM* gene [Cavalieri et al., 2008].

Using MLPA, we identified the c.8851-2kbdel17kb mutation in JPAT3. While it was possible that this LGD mutation was ancestrally related to the previously reported CRAT [B] [Telatar et al., 1998a] and BRAT3 [Mitui et al., 2003] mutations, this now seems unlikely, since all three alleles are carried on different STR haplotypes. Given that homology between repetitive sequences is thought to underlie the formation of some genomic deletions and duplications [Kazazian and Goodier, 2002; Telatar et al., 1998a], we carried out an in silico analysis of DNA sequences flanking genomic deletions and were able to identify several repetitive sequences. The presence of microhomology (GGA in JPAT11) suggests that the recently described microhomology-mediated break-induced replication FoSTeS/MMBIR mechanism could be responsible for generating these deletions [Hastings et al., 2009].

Readthrough of PTCs was first described almost 50 years ago when it was noticed that certain aminoglycosides, such as streptomycin and gentamicin, "suppressed" the mutated phenotype of auxotrophy in strains of *Escherichia coli* suggesting that the drug interfered with accurate translation of the RNA code into protein [Davies et al., 1965]. Later, crystallography studies elegantly demonstrated that aminoglycosides bind to the internal loop of helix 44 (the decoding site) of the 16 S ribosomal RNA [Dibrov et al., 2010; Lynch et al., 2003]. More recently, we identified two new nonaminoglycoside small molecules with readthrough activity on both *ATM* and *dystrophin* genes [Du et al., 2009].

Based on the mutation spectrum of *ATM*, it is estimated that approximately 30% of *ATM* mutations in A-T patients are potentially treatable by mutation-targeted therapy using either RTCs or AMOs. This includes A-T patients who are compound heterozygotes, since RTCs and AMOs restore significant amounts of ATM protein even when only one allele is targeted. We identified three such examples amongst the eight Japanese families. In fact, in vitro, we were able to correct (1) abnormal splicing for JPAT11/12 (Fig. 5A), using a custom-designed AMO to mask the cryptic splice site created by the pseudoexon mutation (c.2639-384A>G); (2) a nonsense mutation in cells from JPAT8/9 using RTCs (Fig. 6). Thus, our results demonstrate that mutation-targeted treatment of cells carrying poorly understood DNA variants can extend our understanding of the consequences of such changes and may also have important therapeutic potential.

Acknowledgments

S.C. received a fellowship from "Associazione Gli Amici di Valentina." We thank Drs. Shareef Nahas, Hailiang Hu, and Mark Ambrose for helpful discussions.

References

Babushok DV, Kazazian HH, Jr. 2007. Progress in understanding the biology of the human mutagen LINE-1. Hum Mutat 28:527–539.

Bakkenist CJ, Kastan MB. 2003. DNA damage activates ATM through intermolecular autophosphorylation and dimer dissociation. Nature 421:499–506.

Birrell GW, Kneebone K, Nefedov M, Nefedova E, Jartsev MN, Mitsui M, Gatti RA, Lavin MF. 2005. ATM mutations, haplotype analysis, and immunological status of Russian patients with ataxia telangiectasia. Hum Mutat 25:593–601.

Boder E, Sedgwick RP. 1958. Ataxia-telangiectasia; a familial syndrome of progressive cerebellar ataxia, oculocutaneous telangiectasia and frequent pulmonary infection. Pediatrics 21:526–554.

Bolderson E, Richard DJ, Zhou BB, Khanna KK. 2009. Recent advances in cancer therapy targeting proteins involved in DNA double-strand break repair. Clin Cancer Res 15:6314–6320.

Broeks A, de Klein A, Floore AN, Muijtjens M, Kleijer WJ, Jaspers NG, van 't Veer LJ. 1998. ATM germline mutations in classical ataxia-telangiectasia patients in the Dutch population. Hum Mutat 12:330–337.

Campbell C, Mitui M, Eng L, Coutinho G, Thorstenson Y, Gatti RA. 2003. ATM mutations on distinct SNP and STR haplotypes in ataxia-telangiectasia patients of differing ethnicities reveal ancestral founder effects. Hum Mutat 21:80–85.

Cartegni L, Wang J, Zhu Z, Zhang MQ, Krainer AR. 2003. ESEfinder: a web resource to identify exonic splicing enhancers. Nucleic Acids Res 31:3568–3571.

Cavalieri S, Funaro A, Pappi P, Migone N, Gatti RA, Brusco A. 2008. Large genomic mutations within the ATM gene detected by MLPA, including a duplication of 41 kb from exon 4 to 20. Ann Hum Genet 72(Pt 1):10–18.

Cavalieri S, Funaro A, Porcedda P, Turinetto V, Migone N, Gatti RA, Brusco A. 2006. ATM mutations in Italian families with ataxia telangiectasia include two distinct large genomic deletions. Hum Mutat 27:1061–1070.

Coutinho G, Mitui M, Campbell C, Costa Carvalho BT, Nahas S, Sun X, Huo Y, Lai CH, Thorstenson Y, Tanouye R, Raskin S, Kim CA, Llerena J Jr, Gatti RA. 2004. Five haplotypes account for fifty-five percent of ATM mutations in Brazilian patients with ataxia telangiectasia: seven new mutations. Am J Med Genet A 126:33–40.

Davies J, Gorini L, Davis BD. 1965. Misreading of RNA codewords induced by aminoglycoside antibiotics. Mol Pharmacol 1:93–106.

Dibrov SM, Parsons J, Hermann T. 2010. A model for the study of ligand binding to the ribosomal RNA helix h44. Nucleic Acids Res 38:4458–4465.

Du L, Damoiseaux R, Nahas S, Gao K, Hu H, Pollard JM, Goldstine J, Jung ME, Henning SM, Bertoni C, Gatti RA. 2009. Nonaminoglycoside compounds induce readthrough of nonsense mutations. J Exp Med 206:2285–2297.

Du L, Kayali R, Bertoni C, Fike F, Hu H, Iversen PL, Gatti RA. 2011. Arginine-rich cell-penetrating peptide dramatically enhances AMO-mediated ATM aberrant splicing correction and enables delivery to brain and cerebellum. Hum Mol Genet 20:3151–3160.

Du L, Lai CH, Concannon P, Gatti RA. 2008. Rapid screen for truncating ATM mutations by PTT-ELISA. Mutat Res 640:139–144.

Du L, Pollard JM, Gatti RA. 2007. Correction of prototypic ATM splicing mutations and aberrant ATM function with antisense morpholino oligonucleotides. Proc Natl Acad Sci USA 104:6007–6012.

Ejima Y, Sasaki MS. 1998. Mutations of the ATM gene detected in Japanese ataxia-telangiectasia patients: possible preponderance of the two founder mutations 4612del165 and 7883del5. Hum Genet 102:403–408.

Eng L, Coutinho G, Nahas S, Yeo G, Tanouye R, Babaei M, Dork T, Burge C, Gatti RA. 2004. Nonclassical splicing mutations in the coding and noncoding regions of the ATM Gene: maximum entropy estimates of splice junction strengths. Hum Mutat 23:67–76.

Fukao T, Song XQ, Yoshida T, Tashita H, Kaneko H, Teramoto T, Inoue R, Katamura K, Mayumi M, Hiratani M and others. 1998. Ataxia-telangiectasia in the Japanese population: identification of R1917X, W2491R, R2909G, IVS33+2T–>A, and 7883del5, the latter two being relatively common mutations. Hum Mutat 12:338–343.

Gatti RA. 2001. Ataxia-telangiectasia. In: Scriver CR, Beaudet AL, Sly WS, Valle D, editors. The Metabolic and Molecular Basis of Inherited Disease. Edition 8. New York: McGraw-Hill 677–704.

Gatti RA, Berkel I, Boder E, Braedt G, Charmley P, Concannon P, Ersoy F, Foroud T, Jaspers NG, Lange K and others. 1988. Localization of an ataxia-telangiectasia gene to chromosome 11q22–23. Nature 336:577–580.

Gilad S, Bar-Shira A, Harnik R, Shkedy D, Ziv Y, Khosravi R, Brown K, Vanagaite L, Xu G, Frydman M, and others. 1996a. Ataxia-telangiectasia: founder effect among north African Jews. Hum Mol Genet 5:2033–2037.

Gilad S, Khosravi R, Shkedy D, Uziel T, Ziv Y, Savitsky K, Rotman G, Smith S, Chessa L, Jorgensen TJ and others. 1996b. Predominance of null mutations in ataxia-telangiectasia. Hum Mol Genet 5:433–439.

Hastings PJ, Ira G, Lupski JR. 2009. A microhomology-mediated break-induced replication model for the origin of human copy number variation. PLoS Genet 5:e1000327.

Kazazian HH, Jr., Goodier JL. 2002. LINE drive. Retrotransposition and genome instability. Cell 110:277–280.

Kozlov SV, Graham ME, Peng C, Chen P, Robinson PJ, Lavin MF. 2006. Involvement of novel autophosphorylation sites in ATM activation. EMBO J 25:3504–3514.

Laake K, Telatar M, Geitvik GA, Hansen RO, Heiberg A, Andresen AM, Gatti R, Borresen-Dale AL. 1998. Identical mutation in 55% of the ATM alleles in 11 Norwegian AT families: evidence for a founder effect. Eur J Hum Genet 6:235–244.

Lai CH, Chun HH, Nahas SA, Mitui M, Gamo KM, Du L, Gatti RA. 2004. Correction of ATM gene function by aminoglycoside-induced read-through of premature termination codons. Proc Natl Acad Sci USA 101:15676–15681.

Lange E, Borresen AL, Chen X, Chessa L, Chiplunkar S, Concannon P, Dandekar S, Gerken S, Lange K, Liang T and others. 1995. Localization of an ataxia-telangiectasia gene to an approximately 500-kb interval on chromosome 11q23.1: linkage analysis of 176 families by an international consortium. Am J Hum Genet 57:112–119.

Liu HX, Cartegni L, Zhang MQ, Krainer AR. 2001. A mechanism for exon skipping caused by nonsense or missense mutations in BRCA1 and other genes. Nat Genet 27:55–58.

Lynch SR, Gonzalez RL, Puglisi JD. 2003. Comparison of X-ray crystal structure of the 30S subunit-antibiotic complex with NMR structure of decoding site oligonucleotide-paromomycin complex. Structure 11:43–53.

Matsuoka S, Ballif BA, Smogorzewska A, McDonald ER, 3rd, Hurov KE, Luo J, Bakalarski CE, Zhao Z, Solimini N, Lerenthal Y and others. 2007. ATM and ATR substrate analysis reveals extensive protein networks responsive to DNA damage. Science 316:1160–1166.

McConville CM, Stankovic T, Byrd PJ, McGuire GM, Yao QY, Lennox GG, Taylor MR. 1996. Mutations associated with variant phenotypes in ataxia-telangiectasia. Am J Hum Genet 59:320–330.

Minegishi Y, Saito M, Morio T, Watanabe K, Agematsu K, Tsuchiya S, Takada H, Hara T, Kawamura N, Ariga T and others. 2006. Human tyrosine kinase 2 deficiency reveals its requisite roles in multiple cytokine signals involved in innate and acquired immunity. Immunity 25:745–755.

Mitui M, Bernatowska E, Pietrucha B, Piotrowska-Jastrzebska J, Eng L, Nahas S, Teraoka S, Sholty G, Purayidom A, Concannon P and others. 2005. ATM gene founder haplotypes and associated mutations in Polish families with ataxia-telangiectasia. Ann Hum Genet 69(Pt 6):657–664.

Mitui M, Campbell C, Coutinho G, Sun X, Lai CH, Thorstenson Y, Castellvi-Bel S, Fernandez L, Monros E, Carvalho BT and others. 2003. Independent mutational events are rare in the ATM gene: haplotype prescreening enhances mutation detection rate. Hum Mutat 22:43–50.

Mitui M, Nahas SA, Du LT, Yang Z, Lai CH, Nakamura K, Arroyo S, Scott S, Purayidom A, Concannon P and others. 2009. Functional and computational assessment of missense variants in the ataxia-telangiectasia mutated (ATM) gene: mutations with increased cancer risk. Hum Mutat 30:12–21.

Morcos PA, Li Y, Jiang S. 2008. Vivo-Morpholinos: a non-peptide transporter delivers Morpholinos into a wide array of mouse tissues. Biotechniques 45:613–614, 616, 618 passim.

Morio T, Takahashi N, Watanabe F, Honda F, Sato M, Takagi M, Imadome K, Miyawaki T, Delia D, Nakamura K and others. 2009. Phenotypic variations between affected siblings with ataxia-telangiectasia: ataxia-telangiectasia in Japan. Int J Hematol 90:455–462.

Moulton JD, Jiang S. 2009. Gene knockdowns in adult animals: PPMOs and vivo-morpholinos. Molecules 14:1304–1323.

Nahas SA, Butch AW, Du L, Gatti RA. 2009. Rapid flow cytometry-based structural maintenance of chromosomes 1 (SMC1) phosphorylation assay for identification of ataxia-telangiectasia homozygotes and heterozygotes. Clin Chem 55:463–472.

Pattison JE. 2004. A comparison of inbreeding rates in India, Japan, Europe and China. HOMO—J Comp Hum Biol 55:113–128.

Savitsky K, Bar-Shira A, Gilad S, Rotman G, Ziv Y, Vanagaite L, Tagle DA, Smith S, Uziel T, Sfez S and others. 1995. A single ataxia telangiectasia gene with a product similar to PI-3 kinase. Science 268:1749–1753.

Schouten JP, McElgunn CJ, Waaijer R, Zwijnenburg D, Diepvens F, Pals G. 2002. Relative quantification of 40 nucleic acid sequences by multiplex ligation-dependent probe amplification. Nucleic Acids Res 30:e57.

Shiloh Y. 2006. The ATM-mediated DNA-damage response: taking shape. Trends Biochem Sci 31:402–410.

Smith PJ, Zhang C, Wang J, Chew SL, Zhang MQ, Krainer AR. 2006. An increased specificity score matrix for the prediction of SF2/ASF-specific exonic splicing enhancers. Hum Mol Genet 15:2490–2508.

Sobeck A. 2001. Caretaker-Gen-Syndrome:Molekulargenetische und Funktionelle Studien. PhD Thesis, Wuerzburg: Julius-Maximilians-University Wuerzburg.

Svedmyr EA, Leibold W, Gatti RA. 1975. Possible use of established cell lines for MLR locus typing. Tissue Antigens 5:186–195.

Telatar M, Teraoka S, Wang Z, Chun HH, Liang T, Castellvi-Bel S, Udar N, Borresen-Dale AL, Chessa L, Bernatowska-Matuszkiewicz E and others. 1998a. Ataxia-telangiectasia: identification and detection of founder-effect mutations in the ATM gene in ethnic populations. Am J Hum Genet 62:86–97.

Telatar M, Wang S, Castellvi-Bel S, Tai LQ, Sheikhavandi S, Regueiro JR, Porras O, Gatti RA. 1998b. A model for ATM heterozygote identification in a large population: four founder-effect ATM mutations identify most of Costa Rican patients with ataxia telangiectasia. Mol Genet Metab 64:36–43.

Teraoka SN, Telatar M, Becker-Catania S, Liang T, Onengut S, Tolun A, Chessa L, Sanal O, Bernatowska E, Gatti RA and others. 1999. Splicing defects in the ataxia-telangiectasia gene, ATM: underlying mutations and consequences. Am J Hum Genet 64:1617–1631.

Udar N, Farzad S, Tai LQ, Bay JO, Gatti RA. 1999. NS22: a highly polymorphic complex microsatellite marker within the ATM gene. Am J Med Genet 82:287–289.

Valentine CR. 1998. The association of nonsense codons with exon skipping. Mutat Res 411:87–117.

Vanagaite L, James MR, Rotman G, Savitsky K, Bar-Shira A, Gilad S, Ziv Y, Uchenik V, Sartiel A, Collins FS and others. 1995. A high-density microsatellite map of the ataxia-telangiectasia locus. Hum Genet 95:451–454.

Westbrook AM, Schiestl RH. 2010. Atm-deficient mice exhibit increased sensitivity to dextran sulfate sodium-induced colitis characterized by elevated DNA damage and persistent immune activation. Cancer Res 70:1875–1884.

Yeo G, Burge CB. 2004. Maximum entropy modeling of short sequence motifs with applications to RNA splicing signals. J Comput Biol 11:377–394.

ELSEVIER

Brain & Development 34 (2012) 287–292

BRAIN & DEVELOPMENT
Official Journal of the Japanese Society of Child Neurology

www.elsevier.com/locate/braindev

Original article

Lesions of cortical GABAergic interneurons and acetylcholine neurons in xeroderma pigmentosum group A

Masaharu Hayashi [a,*], Tatsuyuki Ohto [b], Kei Shioda [c], Ryo Fukatsu [c]

[a] *Department of Brain Development and Neural Regeneration, Tokyo Metropolitan Institute of Medical Science, Tokyo, Japan*
[b] *Department of Pediatrics, Institute of Clinical Medicine, Medical Branch, University of Tsukuba, Ibaraki, Japan*
[c] *Department of Neuropathology, Saitama Medical University, Saitama, Japan*

Received 14 May 2011; received in revised form 28 June 2011; accepted 30 June 2011

Abstract

Xeroderma pigmentosum (XP) is a rare genetic disorder caused by inherited disturbances in the nucleotide excision repair system; patients with XP groups A (XP-A), B, D, and G were shown to have progressive neurological disturbances. Particularly, XP-A patients, which account for approximately half of Japanese XP patients, show severe neurological disorders, including mental retardation and epilepsy. Herein, we performed an immunohistochemical analysis of the number of GABAergic interneurons (GABAis), including calbindin-D28K, parvalbumin, and calretinin, in the cerebral cortex and acetylcholinergic neurons (AchNs) in the nucleus basalis of Meynert (NM) and in the pedunculopontine tegmental nucleus (PPN) in six autopsy cases of XP-A in order to investigate the relationships between mental dysfunction and GABAis and AchNs. The density and percentages of neurons that were immunoreactive for calbindin-D28K and parvalbumin were significantly reduced in the frontal and temporal cortices in XP-A cases, although the density of neurons that were immunoreactive for MAP2 did not differ from that in controls. Additionally, XP-A cases showed reduced AchNs in both the NM and the PPN. The observed reductions of cortical GABAis and AchNs may be involved in the mental disturbances, the higher occurrence of epilepsy, and/or the abnormalities in rapid eye movement sleep in patients with XP-A.
© 2011 The Japanese Society of Child Neurology. Published by Elsevier B.V. All rights reserved.

Keywords: Xeroderma pigmentosum; Mental disabilities; Immunohistochemistry; GABA; Acetylcholine; Nucleus basalis of Meynert; Pedunculopontine tegmental nucleus

1. Introduction

Xeroderma pigmentosum (XP) is a rare genetic disorder caused by inherited disturbances in the nucleotide excision repair (NER) system, and complementation studies using cell hybridization have revealed the existence of 8 XP genes (groups A–G and a variant) [1]. Patients with XP groups A, B, D, and G (XP-A, XP-B, XP-D, and XP-G) exhibit progressive neurological disturbances, and XP-A patients, which account for approximately 55% of XP patients in Japan, demonstrate various and severe neurological disorders [2]. Protection from ultraviolet light can prevent the development of skin symptoms but not the neurological disturbances [3]. Although XP-A cases show widespread neuronal loss throughout the central nervous system (CNS) [4], we found a selective impairment of catecholaminergic neurons (CANs) in the basal ganglia and brainstem in autopsy cases, being related to the occurrence of extrapyramidal symptoms and brainstem dysfunction [5].

* Corresponding author. Tel.: +81 3 6834 2334; fax: +81 3 5316 3150.
E-mail address: hayashi-ms@igakuken.or.jp (M. Hayashi).

0387-7604/$ - see front matter © 2011 The Japanese Society of Child Neurology. Published by Elsevier B.V. All rights reserved.
doi:10.1016/j.braindev.2011.06.015

Calcium-binding proteins, such as calbindin-D28K, parvalbumin, and calretinin, regulate intracellular calcium concentrations in neurons and label nonoverlapping populations of GABAergic interneurons (GABAis) in the CNS. In the cerebral cortex, the GABAis are immunoreactive for each calcium-binding protein. We identified selectively disturbed patterns of calcium-binding protein expression in the cerebral cortex in developmental brain disorders [6–8]. However, acetylcholinergic neurons (AchNs) in the nucleus basalis of Meynert (NM) and the pedunculopontine tegmental nucleus (PPN) are involved in mental development and learning abilities [9]. A lesion of the AchN system was observed in developmental brain disorders, such as Down syndrome and Rett syndrome [10,11].

Patients with XP-A suffer from disturbed mental abilities and a worsening of cerebral atrophy according to computed tomography (CT) or magnetic resonance imaging (MRI) studies [3]. Additionally, Japanese XP-A patients showed a higher incidence of epileptic seizures (approximately 15%) than controls [12]. However, the neuropathological background of cortical dysfunction has not been investigated in detail. We performed an immunohistochemical analysis of GABAis in the cerebral cortex and of AchNs in the MyN and PPN in six autopsy cases of XP-A and confirmed that lesions of GABAis and AchNs are involved in the mental abnormalities exhibited by these patients.

2. Materials and methods

2.1. Subjects

Clinical subjects included six cases of clinically and genetically confirmed XP-A and 5 controls with no pathological changes in the central nervous system; subjects were aged from 9 to 47 years (Table 1). Clinical findings in XP-A cases 1–2 and 4–6 were reported previously [4]. The ethical committee of the Tokyo Metropolitan Institute of Medical Science approved this study, and the family of each subject provided informed consent for the postmortem analysis.

2.2. Immunohistochemistry

Brains were fixed in a buffered formalin solution. Each formalin-fixed brain was cut coronally and then embedded in paraffin. Six-μm-thick serial sections were cut from selected brain regions, including the superior frontal cortex, the middle temporal cortex, the hypothalamus including the NM, and the lower midbrain including the PPN. After microwave antigen retrieval, each section was treated with mouse monoclonal antibodies to microtubule-associated protein 2 (MAP2; 1:100, Upstate Cell Signaling Solutions, Billerica, MA, USA), acetylcholinesterase (AchE; Affinity Bioreagents, Inc., Golden, CO, USA), tyrosine hydroxylase (TH; Affinity Bioreagents, Inc.), parvalbumin (PV; Novocastra Laboratories, Newcastle upon Tyne, UK), calbindin-D28K (CD; Novocastra Laboratories), and calretinin (CR; Novocastra Laboratories) at the following concentrations: 1:100 (MAP2, PV, CD, and CR), 1:250 (AchE), and 1:400 (TH). Antibody binding was visualized using the avidin–biotin-immunoperoxidase complex method (Nichirei, Tokyo, Japan) according to the manufacturer's protocol. No staining was detected in the sections in the absence of antibody.

2.3. Quantitative evaluation and data analysis

From the second to the fourth layers in the cerebral cortex, the number of cells immunoreactive for MAP2 and each calcium-binding protein was counted in 6 nonoverlapping microscopic subfields at a 100-fold magnification using a counting box (1 mm^2) to obtain the density of immunoreactive cells. The percentages of cells immunoreactive for each calcium-binding protein relative to those immunoreactive for MAP2 were also

Table 1
Summary of subjects.

	Age (years)	Sex	Cause of death	Post-mortem time (h)	Brain weight (g)
	Controls				
1	9	Male	Acute leukemia	4	n/A
2	16	Male	Pneumonia	6	1505
3	29	Female	Guilain-Barre syndrome	4	n/A
4	36	Female	Thrombotic thromcytopenic purpura	2	1475
5	47	Male	Acute leukemia	10	1400
	Xeroderma pigmentosum group A				
1	19	Male	Candidiasis	2	580
2	19	Male	Renal failure	2	610
3	21	Male	Pneumonia	18	720
4	23	Female	Pneumonia	9	580
5	24	Female	Pneumonia	4	500
6	26	Female	Pneumonia	5	530

Abbreviations: N/A, not accessed.

calculated. In the NM, all AchE-immunoreactive cells were counted ventral to the globus pallidus. The PPN was identified dorsolateral to the rostral superior cerebellar peduncle and the medial lemniscus in the lower midbrain, following the atlas of Olszewski and Baxter [13]. The PPN is composed of clusters of moderately large neurons (pars compacta) and the more widespread pars dissipata in the rostral and medial regions [9]. In the pars compacta of the PPN, the number of cells immunoreactive for MAP2, AchE, TH, and CD were determined after the manual labeling of appropriate cells with nucleoli in 2 serial sections, and the mean value was calculated. The percentages of cells immunoreactive for AchE, TH, and CD relative to those immunoreactive for MAP2 were also calculated. All data are presented as the mean ± SD and analyzed using the nonparametric Mann–Whitney *U* test in order to compare the results between the XPA cases and controls for a quantitative evaluation of immunoreactive cells. The level of significance was set at $P < 0.05$ to adjust for comparisons.

3. Results

In the cerebral cortex, interneurons immunoreactive for CD, PV, and CR were identified in the second and third layers, near the fourth layer, and from the second to the fourth layers, respectively (Fig. 1A). The density of neurons immunoreactive for MAP2 in the superior frontal cortex and inferior temporal cortex in cases of XP-A did not differ from the average density of that in controls (Table 2). Nevertheless, the density and percentages of neurons immunoreactive for both CD and PV was significantly reduced in the frontal and temporal cortices in cases of XP-A (Fig. 1B). The number and percentage of neurons immunoreactive for CR were reduced in the middle temporal cortex, whereas these values were comparatively preserved in the superior frontal cortex (Table 2). The data suggest a selective impairment of GABAis in the cerebral cortex in cases of XP-A. In the NM, the mean ± SD of the total number of neurons immunoreactive for AchE was 91.7 ± 25.7 in controls (Fig. 1C), and that in XP-A cases was 0.4 ± 0.8, indicating a significant loss of AchNs ($P < 0.01$) (Fig. 1D). In the PPN, the number of neurons immunoreactive for MAP2 in cases of XP-A was reduced to fewer than half of those in controls (Table 3). The numbers and percentages of both AchNs and CANs, which are immunoreactive for AchE and TH (Fig. 1E and F), respectively, were reduced in XP-A cases (Table 3), whereas those immunoreactive for CD remained consistent.

4. Discussion

We previously reported a reduction of CD- and PV-immunoreactive GABAis in the cerebral cortex in samples from patients with various developmental disorders, including neuronal ceroid lipofuscinosis (NCL) [6], dentatorubral–pallidoluysian atrophy (DRPLA) [8], and mucopolysaccharidosis (MPS) [7]. This reduction may be related to the epileptogenesis of progressive myoclonic epilepsy in NCL and DRPLA and the mental disabilities in MPS, respectively. A similar reduction of CD- and PV-immunoreactive GABAis in the cerebral cortex was observed in XP-A cases. XP-A cases exhibited severe brain atrophy (Table 1), and the total number of cerebral neurons was lower than that in controls. However, there was no difference in the density of neurons immunoreactive for MAP2 between controls and XP-A cases (Table 2).

We previously reported that neuronal loss was observed throughout the cerebral cortex in cases of XP-A, and there was no difference in the density of the remaining pyramidal cells between the layers [4]. However, this analysis demonstrated that GABAis are more vulnerable than pyramidal neurons from the second layer to the fourth layers in the cerebral cortex. Evaluating neuronal loss in the brain according to individual subgroups is important for XP-A cases, although the lesion appears to be diffuse and extensive. It is known that GABA receptor-mediated postsynaptic inhibition has important roles in normal cortical function and in controlling events implicated in epileptogenesis, and the decreases in numbers of GABAis and/or postsynaptic inhibition have been reported in the epileptogenic hippocampus and neocortex [14]. The selective loss of CD- and PV-immunoreactive cells was reported in the temporal cortex in Alzheimer's disease and in the prefrontal cortex in schizophrenia [15,16]. The reduction of inhibitory GABAis may be involved in the progressive mental disturbances and the higher occurrence of epilepsyin patients with XP-A. Concurrently, GABAergic anticonvulsants should be used carefully in patients considering the selective reduction of GABAis in the cerebral cortex.

PPN, which is in the lower midbrain, contains cholinergic and noncholinergic neurons and has afferent and efferent connections to the basal ganglia and spinal cord. The cholinergic innervation from the PPN to the thalamus and pons is involved in the generation of muscle tone and rapid eye movement (REM) sleep, and the PPN is believed to be a part of the mesencephalic locomotor region [17]. In controls, there was an age-dependent change in the percentages of AchNs and CANs in the PPN. Cases of perinatal brain damage showed a reduced percentage of AchNs with a compensatory increased percentage of CANs [9]. AchNs were reduced in the PPN in patients with Prader–Willi syndrome, although GABAis in the cerebral cortex, in addition to AchN in the NM, were relatively well-preserved [18].

This analysis revealed a severe reduction in the percentage of AchNs and CANs in the PPN in cases of

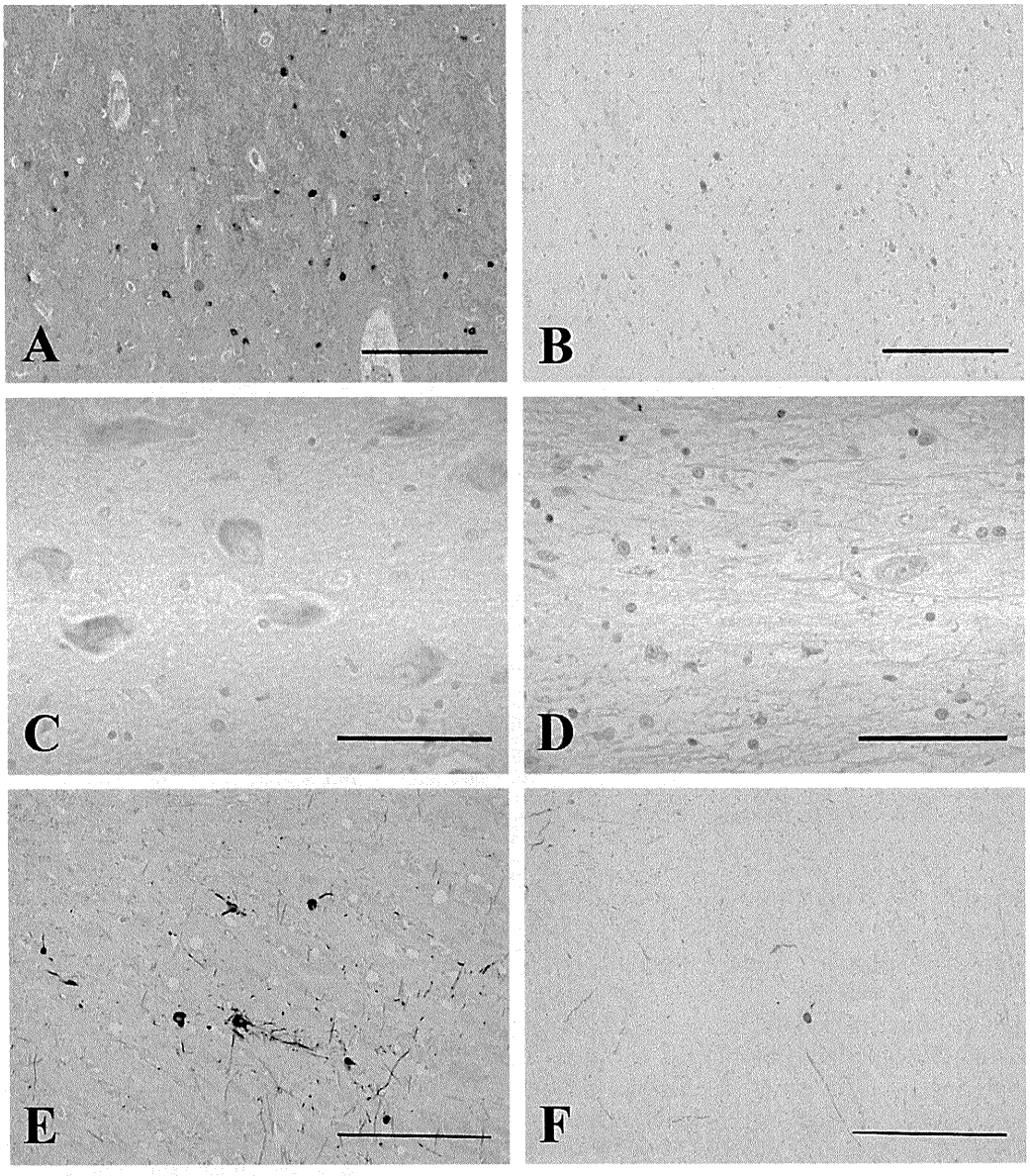

Fig. 1. Representative illustrations of immunohistochemistry in controls and cases of xeroderma pigmentosum group A (XP-A). Immunoreactivities for parvalbumin were found in the interneurons and neuropil around the fourth layer of frontal cortex in control 2 (A), whereas those were reduced in XP-A case 2 (B). Bars = 200 μm. Neurons with cytoplasmic granules immunoreactive for acetylcholine esterase were observed in the nucleus basalis of Meynert in control 3 (C) but not in XP-A case 3 (D). Bars = 100 μm. The pedunculopontine tegmental nucleus had neurons and neuronal processes immunoreactive for tyrosine hydroxylase in control 2 (E), which were reduced in XP-A case 3 (F). Bars = 400 μm.

XP-A, whereas GABAis immunoreactive for CD were relatively spared (Table 3). Unlike the AchNs in Prader-Willi syndrome [18], AchNs were also damaged in the NM. Impairment of CANs seem to occur throughout the CNS, given the reduction of CAN in the basal ganglia and brainstem that we reported previously [5]. Interestingly, a disturbance of motor inhibition during REM sleep was identified in patients with XP-A [19]. Damage of the monoaminergic neurons in the brainstem, including the PPN, may be involved in abnormalities of muscle tone and/or REM sleep, in addition to mental disturbances in patients with XP-A. Recently, we reported successful treatment with low-dose levodopa for laryngeal dystonia, from which many aged patients with XP-A generally suffer [20]. Low-dose levodopa is thought to alleviate dopamine receptor supersensitivity in the basal ganglia. Treatment with donepezil, an acetylcholinergic agent, corrected REM sleep abnormalities in patients with Alzheimer's disease [21] and ameliorated REM sleep behavior disorders in cases of dementia with Lewy bodies [22]. Recently, donepezil has been tested in young adults with Down syndrome [23], in which AchNs were impaired [10,11]. Scores in modified International Classification of

Table 2
Summary of quantitative analysis in the cerebral cortex.

		Superior frontal cortex			Middle temporal cortex		
		Controls (mean ± SD)	XP-A (mean ± SD)	Mann–Whitney test (p value)	Controls (mean ± SD)	XP-A (mean ± SD)	Mann–Whitney test (p value)
Microtubule associated protein 2		122 ± 13	121 ± 2	ns	124 ± 8	110 ± 8	ns
Calbindin-D28K		33 ± 7	8 ± 7	<0.01	33 ± 4	9 ± 4	<0.01
	(%)	31 ± 5	12 ± 12	<0.05	27 ± 4	8 ± 3	<0.01
Parvalbumin		27 ± 4	15 ± 10	<0.05	22 ± 1	5 ± 4	<0.01
	(%)	26 ± 2	12 ± 8	<0.05	17 ± 2	5 ± 3	<0.01
Calretinin		49 ± 5	44 ± 11	ns	50 ± 7	36 ± 6	<0.05
	(%)	42 ± 5	36 ± 9	ns	41 ± 4	32 ± 5	<0.05

Abbreviations: XP-A, xeroderma pigmentosum group A; ns, not significant.

Table 3
Summary of quantitative analysis in the pedunculopontine tegmental nucleus.

		Controls (mean ± SD)	XP-A (mean ± SD)	Mann–Whitney test (p value)
Microtubule associated protein 2		244 ± 44.5	96 ± 16	<0.01
Acetylcholine esterase		68.2 ± 18	0	<0.01
	(%)	29 ± 9.6	0.2 ± 0.4	<0.01
Tyrosine hydroxylase		24.8 ± 14.6	3.4 ± 2.8	<0.01
	(%)	10.2 ± 4.8	3.3 ± 2.5	<0.05
Calbindin-D28K		26.8 ± 18.2	20 ± 12	ns
	(%)	10.7 ± 6.9	20.1 ± 12.3	ns

Abbreviations: XP-A, xeroderma pigmentosum group A; ns, not significant.

Functioning, Disability and Health scaling system significantly increased without any adverse effects in patients with Down syndrome treated with donepezil in comparison to those in placebo controls in a 24-week randomized, double-blind, placebo-controlled trial [24]. We hypothesize that donepezil may be effective for treating mental disturbances and/or REM sleep abnormalities in patients with XP-A, although donepezil has never been used in these patients.

The pathogenesis of the lesions of the cortical GABAis and AchNs in cases of XP-Ais not clear. We observed the involvement of apoptotic neuronal loss and oxidative stress with disturbed glutamate transport in the degeneration of the cerebellar cortex and the basal ganglia, respectively, in XP-A [25–27]. However, neither apoptotic neuronal loss nor oxidative stress was observed in the cerebral cortex, the NM, or the PPN. It is possible that the disturbed NER and/or null expression of XP-A protein may affect the development and/or survival of specific neuronal groups in the brain. Nevertheless, *Xpa* gene-knockout mice, an animal model of XP-A, are deficient in NER and sensitive to ultraviolet-induced skin carcinogenesis, but they are behaviorally normal and lack significant neuronal loss in the brain [28]. Further research in mice using a conditional knock-out of the *Xpa* gene in the brain may be helpful to clarify the pathogenesis of the impairment of specific neuron groups in XP-A.

References

[1] Kraemer KH, Patronas NJ, Schiffmann R, Brooks BP, Tamura D, Digiovanna JJ. Xeroderma pigmentosum, trichothiodystrophy and Cockayne syndrome: a complex genotype–phenotype relationship. Neuroscience 2007;145:1388–96.
[2] Hirai Y, Kodama Y, Moriwaki S, Noda A, Cullings HM, Macphess DG, et al. Heterozygous individuals bearing a founder mutation in the XPA DNA repair gene comprise nearly 1% of the Japanese population. Mutat Res 2006;601:171–8.
[3] Hayashi M. Role of oxidative stress in xeroderma pigmentosum. Adv Exp Med Biol 2008;637:120–7.
[4] Itoh M, Hayashi M, Shioda K, Minagawa M, Isa F, Tamagawa K, et al. Neurodegeneration in hereditary nucleotide repair disorders. Brain Dev 1999;21:326–33.
[5] Hayashi M, Araki S, Kohyama J, Shioda K, Fukatsu R, Tamagawa K. Brainstem and basal ganglia lesions in xeroderma pigmentosum group A. J Neuropathol Exp Neurol 2004;63:1048–57.
[6] Hachiya Y, Hayashi M, Kumada S, Uchiyama A, Tsuchiya K, Kurata K. Mechanisms of neurodegeneration in neuronal ceroid-lipofuscinosis. Acta Neuropathol 2006;111:168–77.
[7] Hamano K, Hayashi M, Shioda K, Fukatasu R, Mizutani S. Mechanisms of neurodegeneration in mucopolysaccharidoses II and IIIB: analysis of human brain tissue. Acta Neuropathol 2008;115:547–59.
[8] Hayashi M, Kumada S, Shioda K, Fukatsu R. Neuropathological analysis of the brainstem and cerebral cortex lesions on epileptogenesis in hereditary dentatorubral-pallidoluysian atrophy. Brain Dev 2007;29:473–81.
[9] Anzai Y, Hayashi M, Ohya T, Yokota S. The pedunculopontine nucleus in developmental disorders of the basal ganglia. Neuropathology 2008;28:258–63.

[10] Isacson O, Seo H, Lin L, Albeck D, Granholm AC. Alzheimer's disease and Down's syndrome: roles of APP, trophic factors and Ach. Trends Neurosci 2002;25:79–84.
[11] Berger-Sweeney J. The cholinergic basal forebrain system during development and its influence on cognitive processes: important questions and potential answers. Neurosci Biobehav Rev 2003;27:401–11.
[12] Kohyama J, Furushima W, Sugawara Y, Shimohira M, Hasegawa T, Hayashi M, et al. Convulsive episodes in patients with group A xeroderma pigmentosum. Acta Scand Neurol 2005;112:265–9.
[13] Olszewski J, Baxter D. Cytoarchitecture of the human brain stem. 2nd ed. New York: Karger; 1982.
[14] Prince DA, Parada I, Scalise K, Graber K, Shen F. Epilepsy following cortical injury: cellular and molecular mechanisms as targets for potential prophylaxis. Epilepsia 2009;50:30–40.
[15] Mikkonen M, Alafuzoff I, Tapiola T, Soininen H, Miettinen R. Subfield- and layer-specific changes in parvalbumin, calretinin, and calbindin-D28K immunoreactivity in the entorhinal cortex in Alzheimer's disease. Neuroscience 1999;92:515–32.
[16] Beasley CL, Zhang ZJ, Patten I, Reynolds GP. Selective deficits in prefrontal cortical GABAergic neurons in schizophrenia defined by the presence of calcium-binding proteins. Biol Psychiatry 2002;52:708–15.
[17] Lee MS, Rinne JO, Marsden CD. The pedunculopontine nucleus: its role in the genesis of movement disorders. Yonsei Med J 2000;41:167–84.
[18] Hayashi M, Miyata R, Tanuma N. Decrease in acetylcholinergic neurons in the pedunculopontine tegmental nucleus in a patient with Prader-Willi syndrome. Neuropathology 2011;31:280–5.
[19] Kohyama J, Shimohira M, Kondo S, Fukuro S, Kouji T, Sugimoto J, et al. Motor disturbances during REM sleep in group A xeroderma pigmentosum. Acta Neurol Scand 1995;92:91–5.
[20] Miyata R, Sasaki T, Hayashi M, Araki S, Shimohira M, Kohyama J. Low dose of levodopa is effective for laryngeal dystonia in xeroderma pigmentosum group A. Brain Dev 2010;32:685–7.
[21] MoraesWdos S, Povares DR, Guilleminault C, Ramos LR, Bertolucci PH, Tufik S. The effect of donepezil on sleep and REM sleep EEG in patients with Alzheimer disease: a double-blind placebo-controlled study. Sleep 2006;29:199–205.
[22] Massironi G, Galluzzi S, Frisoni GB. Drug treatment of REM sleep behavior disorders in dementia with Lewy bodies. Int Psychogeriatr 2003;15:377–83.
[23] Kishnani PS, Sommer BR, Handen BL, Seltzer B, Capone GT, Spiridigliozzi GA, et al. The efficacy, safety, and tolerability of donepezil for the treatment of young adults with Down syndrome. Am J Med Genet A 2009;149A:1641–54.
[24] Kondoh T, Kanno A, Itoh H, Nakashima M, Honda R, Kojima M, et al. Donepezil significantly improves abilities in daily lives of female Down syndrome patients with severe cognitive impairment: a 24-week randomized, double-blind, placebo-controlled trial. Int J Psychiatry Med 2011;41:71–89.
[25] Kohji T, Hayashi M, Shioda K, Minagawa M, Morimatsu Y, Tamagawa K, et al. Cerebellar neurodegeneration in human hereditary DNA repair disorders. Neurosci Lett 1998;243:133–6.
[26] Hayashi M, Itoh M, Araki S, Kumada S, Shioda K, Tamagawa K, et al. Oxidative stress and glutamate transport in hereditary nucleotide repair disorders. J Neuropathol Exp Neurol 2001;60:350–6.
[27] Hayashi M, Araki S, Kohyama J, Shioda K, Fukatsu R. Oxidative nucleotide damage and superoxide dismutase expression in the brains of xeroderma pigmentosum group A and Cockayne syndrome. Brain Dev 2005;27:34–8.
[28] Nakane H, Hirota S, Brooks PJ, Nakabeppu Y, Nakatsu Y, Nishimune Y, et al. Impaired spermatogenesis and elevated spontaneous tumorigenesis in xeroderma pigmentosum group A gene (Xpa)-deficient mice. DNA Repair 2008;7:1938–50.

NEUROPATHOLOGY

Neuropathology 2011; ••, ••–••

doi:10.1111/j.1440-1789.2011.01241.x

Original Article

Brain vascular changes in Cockayne syndrome

Masaharu Hayashi,[1] Naho Miwa-Saito,[1] Naoyuki Tanuma[1] and Masaya Kubota[2]

[1]Department of Brain Development and Neural Regeneration, Tokyo Metropolitan Institute of Medical Science and [2]Department of Neurology, National Center for Child Health and Development, Tokyo, Japan

Cockayne syndrome (CS) and xeroderma pigmentosum (XP) are caused by deficient nucleotide excision repair. CS is characterized by cachectic dwarfism, mental disability, microcephaly and progeria features. Neuropathological examination of CS patients reveals dysmyelination and basal ganglia calcification. In addition, arteriosclerosis in the brain and subdural hemorrhage have been reported in a few CS cases. Herein, we performed elastica van Gieson (EVG) staining and immunohistochemistry for collagen type IV, CD34 and aquaporin 4 to evaluate the brain vessels in autopsy cases of CS, XP group A (XP-A) and controls. Small arteries without arteriosclerosis in the subarachnoid space had increased in CS cases but not in either XP-A cases or controls. In addition, string vessels (twisted capillaries) in the cerebral white matter and increased density of CD34-immunoreactive vessels were observed in CS cases. Immunohistochemistry findings for aquaporin 4 indicated no pathological changes in either CS or XP-A cases. Hence, the increased subarachnoid artery space may have caused subdural hemorrhage. Since such vascular changes were not observed in XP-A cases, the increased density of vessels in CS cases was not caused by brain atrophy. Hence, brain vascular changes may be involved in neurological disturbances in CS.

Key words: brain vessels, CD34, Cockayne syndrome, immunohistochemistry, xeroderma pigmentosum.

INTRODUCTION

Cockayne syndrome (CS) is a rare genetic disorder caused by deficient nucleotide excision repair (NER), and it is characterized by cachectic dwarfism, mental disability, microcephaly, cerebellar ataxia, retinal pigmentation, and neural deafness.[1] Neuropathological findings of CS patients show small cerebrum, tigroid leukoencephalopathy (dysmyelination), basal ganglia calcification, cerebellar atrophy and demyelinating peripheral neuropathy.[2] Many features of CS resemble those of premature aging, and hence, CS is considered as a progeroid syndrome.[3] Nancy and Berry divided 140 published cases into three types: type I, the most prevalent classical childhood disorder; type II, an infrequent, severe congenital, or infantile variant of the disorder; type III, atypical late onset of the disorder with prolonged survival.[4]

Xeroderma pigmentosum (XP) is an inherited neurocutaneous disorder caused by defects in the NER system.[1] Complementation studies using cell hybridization assays revealed the existence of eight genes in XP (groups A–G and a variant) and two in CS (A and B). NER includes global genome repair and transcription-coupled repair (TCR), which involves several XP genes (especially *XP-A* to *XP-G*) and two CS genes (*CSA* and *CSB*). In XP, the initial presentations are skin symptoms and progressive neurological manifestations, including cognitive and motor deterioration, neuronal deafness, peripheral neuropathy and brain atrophy, mainly in XP-A, XP-B, XP-D and XP-G cases.[2] The molecular basis of CS includes recessive mutations in *CSA* (*CKN1* or *ERCC8*) and *CSB* (*CKN2* or *ERCC6*) genes, but it has not been systematically mapped to the clinical phenotypes. We investigated neurodegeneration in autopsy cases of CS and XP-A.[2]

Arteriosclerosis in the brain[5] and cerebral vascular disorders have been reported in a few cases.[6] In order to characterize the brain vascular changes in CS, we compared the immunohistochemical changes in the brain vessels between CS cases and XP-A cases as disease controls.

MATERIALS AND METHODS

Subjects

The clinical study comprised five cases of clinically and genetically confirmed CS, six cases of clinically and

Correspondence: Masaharu Hayashi, Project Leader, Department of Brain Development and Neural Regeneration, Tokyo Metropolitan Institute of Medical Science, 2-1-6, Kamikitazawa, Setagaya-ku, Tokyo 156-8506, Japan. Email: hayashi-ms@igakuken.or.jp

Received 16 May 2011; revised and accepted 31 May 2011.

© 2011 Japanese Society of Neuropathology

Table 1 Summary of brain vascular changes in subjects

Subject	Age (years)	Sex	Cause of death	Brain weight (g)	Increase of subarachnoid small arteries	Twisted capillaries in the white matter	Density of CD34-immunoreactive vessels	
							Frontal Mean (SD)	Temporal Mean (SD)
Controls								
1	9	Male	Acute leukemia	N/A	(−)	(−)	29 (2)	21 (5)
2	13	Male	Chronic hepatitis	n/A	(−)	(−)	31 (1)	N/A
3	16	Male	Pneumonia	1505	(−)	(−)	29 (3)	25 (1)
4	20	Male	Malignant hyperthermia	N/A	(−)	(−)	26 (2)	25 (5)
5	29	Female	Guilain-Barre syndrome	N/A	(−)	(−)	38 (3)	33 (6)
6	36	Female	Thrombotic thrombocytopenic purpura	1475	(−)	(−)	37 (1)	30 (4)
7	47	Male	Acute leukemia	1400	(−)	(−)	35 (5)	38 (3)
8	55	Male	Lung cancer	N/A	(−)	(−)	38 (3)	36 (4)
9	60	Female	Breast cancer	1080	(−)	(−)	41 (7)	43 (4)
10	71	Male	Lung cancer	N/A	(−)	(−)	49 (3)	41 (4)
Cockayne syndrome								
1	7	Female	Pneumonia	295	1+	1+	44 (4)	41 (2)
2	15	Male	Renal failure	340	1+	1+	45 (4)	43 (4)
3	16	Female	Asthma	615	1+	(−)	48 (6)	N/A
4	18	Male	Renal failure	400	1+	1+	53 (5)	49 (5)
5	18	Male	Renal failure	414	1+	1+	44 (5)	45 (4)
Xeroderma pigmentosum group A								
1	19	Male	Candidiasis	580	(−)	(−)	28 (7)	26 (3)
2	19	Male	Renal failure	610	(−)	(−)	29 (11)	27 (2)
3	21	Male	Pneumonia	720	(−)	(−)	28 (3)	28 (2)
4	23	Female	Pneumonia	580	(−)	(−)	32 (2)	30 (3)
5	24	Female	Pneumonia	500	(−)	(−)	39 (4)	38 (4)
6	26	Female	Pneumonia	530	(−)	(−)	39 (3)	38 (4)

N/A, not assessed.

genetically confirmed XP-A, and 10 controls without any pathological changes in the CNS, aged 9–71 years (Table 1). The clinical and pathological findings in the CS cases 1–4 and XP-A cases 1–2 and 4–6 were reported previously.[7] The study was approved by the ethical committee of Tokyo Metropolitan Institute of Medical Science; informed consent was obtained from the patients' families before performing post mortem analyses.

Histochemistry and immunohistochemistry

The brains were fixed in buffered formalin solution; coronal sections of each formalin-fixed brain sample were cut and embedded in paraffin. Serial 6-μm-thick sections were cut from selected brain regions, including the superior frontal cortex, middle temporal cortex, basal ganglia and thalamus. HE staining and elastica van Gieson (EVG) staining were performed. After microwave antigen retrieval, each section was treated with CD34 (Nichirei, Tokyo, Japan) and rabbit polyclonal antibody to aquaporin 4 (AQP4; Santa Cruz Biotech, Santa Cruz, CA, USA). Each section was pretreated with proteinase K and mouse monoclonal antibody to collagen type IV (Col4: Sigma-Aldrich, St Louis, MO, USA). The antibody concentrations used for analysis were as follows: 1:1 (CD34), 1:100 (AQP4) and 1:500 (Col4). Antibody binding was visualized by means of the avidin–biotin immunoperoxidase complex method (Nichirei, Tokyo, Japan) according to the manufacturer's protocol.

Quantitative evaluation and data analysis

To determine the densities of the immunoreactive vessels, including arteries, veins and capillaries in the superior frontal cortex and middle temporal cortex, we determined the numbers of vessels immunoreactive for CD34 in five nonoverlapping microscopic subfields at 200-fold magnification by using a counting box (0.5 mm^2). Data were presented as mean (SD) and analyzed by nonparametric Mann–Whitney *U*-test to compare the results in different subjects. The level of significance was set at $P < 0.05$ to adjust for comparisons.

RESULTS

The results of HE and EVG staining and immunohistochemistry suggested that only CS patients had increased small arteries and arterioles in the subarachnoid space filled with fibrotic tissue and without arteriosclerosis (Table 1 and Fig. 1A). Further, small twisted and longitudinally running capillaries in cerebral white matter were observed in 4/5 CS patients but were not found in the brain

© 2011 Japanese Society of Neuropathology

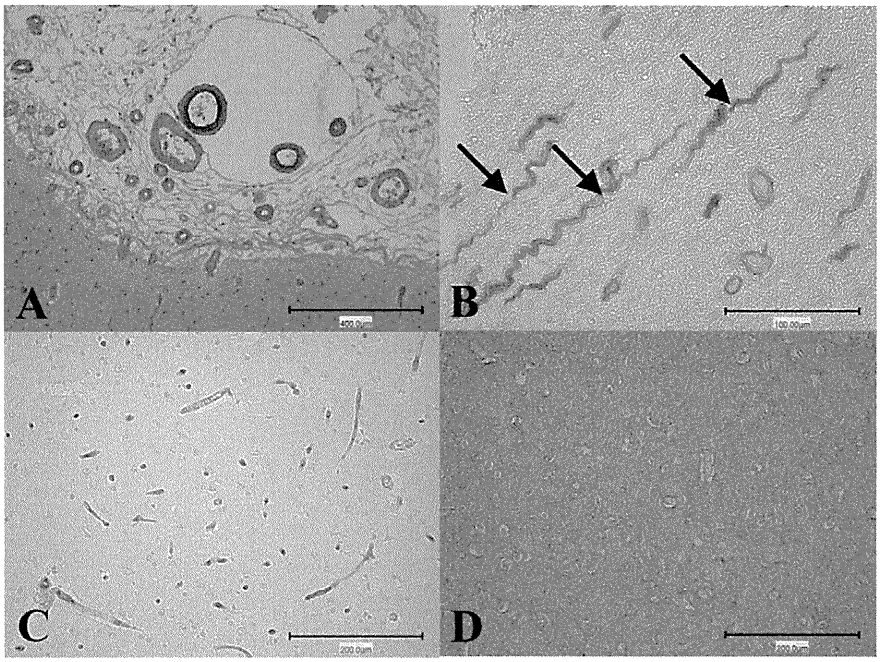

Fig. 1 Vascular changes in the brain of Cockayne syndrome (CS) patients. (A) Small arteries had increased subarachnoid space in CS case 1, elastica van Gieson staining. Bar = 400 μm. (B) Small twisted capillaries (arrows) were identified by immunostaining for collagen type IV in the cerebral white matter in CS case 4. Bar = 100 μm. (C) Vessels immunoreactive for CD34 in the middle temporal cortex in CS case 2. Bar = 200 μm. (D) Astrocyte processes were diffusely visualized by immunohistochemistry for aquaporin 4 in the cerebral white matter in CS case 4. Bar = 200 μm.

in either XP-A patients or controls (Table 1 and Fig. 1B). Twisted capillaries had more than five undulations, and were differentiated from functioning capillaries. In controls, the density of CD34-immunoreactive vessels in the frontal and temporal cortex of aged subjects was one-and-half times higher than that in teenagers, suggesting that the increase was age-dependent (Table 1). The density of CD34-immunoreactive vessels in CS cases aged less than 20 years was over 40 (Fig. 1C), which was equal to that in aged controls. The mean (SD) was 32 (4) in controls aged from 9 to 36 years, 47 (3) in CS cases, and 33 (5) in XP-A cases in the superior frontal cortex, respectively. The mean (SD) was 27 (4) in controls aged from 9 to 36 years, 45 (3) in CS cases, and 31 (5) in XP-A cases in the middle temporal cortex, respectively. The density of CD34-immunoreactive vessels in CS cases was significantly higher than those in controls and XP-A patients ($P < 0.05$). Furthermore, in CS patients, the number of capillaries increased around the calcified foci in the basal ganglia (data not shown). The vessel wall calcification was not found in the cerebral cortex, white matter or subarachnoid space. AQP4 immunostaining visualized the astrocyte processes around the vessels in all subjects (Fig. 1D) and there were no pathological changes in either CS or XP-A patients.

DISCUSSION

Cockayne syndrome and XP-A patients had severe brain atrophy (Table 1) and fibrosis in the enlarged subarachnoid space. However, the number of arteries and arterioles increased only in CS patients, suggesting excessive branching in the cortical arteries in CS. Similarly, in the subarachnoid space, increased density of CD34-immunoreactive vessels in the frontal and temporal cortex was observed in CS but not in XP-A patients. The reduction of brain area due to brain atrophy possibly leads to the apparent increase in the density of vessels. Nevertheless, since there was no increase in density in XP-A patients, the increased density of vessels in CS patients was not caused by the brain atrophy. Subdural hemorrhage is usually caused by tearing of the bridging cortical veins after head trauma, but traumatic aneurysms in the cortical arteries are a rare cause of such hemorrhages.[8] The increased number of subarachnoid and/or intracortical arteries may be a risk factor for subdural hemorrhage, which has been reported in CS patients.[6] A recent study showed that *CSB* mutant cells did not exhibit a normal reaction to hypoxia; these cells did not activate hypoxia-inducible factor-1 on the promoter gene due to which downstream events such as transcription factor IIB (TFIIB) recruitment did not occur.[9] Insufficient hypoxic response may disturb the induction of growth factors such as VEGF, suggesting the possible involvement of angiogenesis in CS. The analysis of brain vessels in fetal autopsy cases of CS might reveal the disturbances of angiogenesis during brain development.

Rapin *et al.* reported twisted microvessels consistent with so-called string vessels in the brains of adult CS patients.[5] We observed a similar morphological change in CS patients in our analysis. The absence of twisted microvessels in XP-A patients is noteworthy, and deficient NER is unlikely to have direct relationships with the

© 2011 Japanese Society of Neuropathology

vascular changes in CS patients. Brooks *et al.* stressed that in addition to brain vascular lesions, there is an overlap in neurological symptoms, such as dysmyelination and brain calcification between CS and Aicardi–Goutières syndrome. They proposed that the vascular changes probably occur due to alterations in gene expression and may play a role in the generation of neurological abnormalities in both the diseases.[10]

CS is considered to be a progeroid condition since many symptoms of CS resemble premature aging. It is intriguing that arteriosclerosis was absent in the brain vessels in our CS patients, although this change has been pointed out in CS cases reported in the literature. In good accordance of our findings, the absence of atherosclerotic changes in the systemic arteries was reported in a 40-year-old patient with CS of probable type III.[11] Furthermore, neither senile plaques nor vascular beta-amyloid depositions were identified in the temporal lobe in three patients with CS of probably type I or II, two aged 2 and one aged 6 years, respectively.[12] In Werner syndrome (WS) associated with supposed accelerated aging, patients rarely show age-associated neuropathology and lack amyloid deposition, indicating the absence of extension of WS-associated aging in the CNS.[13] Although the increased occurrence of arteriosclerosis in the heart, aorta and kidney is a definite characteristic of CS and WS, further analysis of many autopsy cases is required to verify the facilitation of brain arteriosclerosis in both the disorders.

Mouse models for CS-A and CS-B show a TCR defect and increased photosensitivity in the skin. However, growth failure and neurological abnormalities are not predominant.[14,15] $Csb^{m/m}/Xpa^{-/-}$ double mutant animals show post natal growth retardation, ataxia, abnormal locomotor activity, progressive weight loss and early death.[16] However, in these model animals, brain vascular changes have not been examined in detail. Complete inactivation of NER by deletion of *XP-A* gene in animals does not cause CS-like neurodevelopmental and progeroid features, and it has been proposed that some of the CS features may be the outcome of defects in the transcription function of transcription/repair factor TFIIH and/or defective repair of oxidative DNA lesions.[17] We have investigated the involvement of oxidative stress in the brains of XP-A and CS autopsy cases.[2] Lipid peroxidation and protein glycation markers were found in the perivascular calcification areas in the globus pallidus and cerebellum more predominantly in CS than in XP-A patients. We found a similar deposition of oxidative stress markers in the calcification areas in the brain vessel walls in cases of pseudohypoparathyroidism and Fahr disease.[18] Since increased oxidative stress is known to cause vascular calcifications in bone and kidney diseases,[19,20] it is possible that oxidative stress may be involved in the generation of brain vascular changes in CS.

Our findings suggest that vascular changes in the brain may be involved in neurological disturbances in CS. A detailed investigation of the brain vessels may help us clarify the pathogenesis of neurological abnormalities.

REFERENCES

1. Kraemer KH, Patronas NJ, Schiffmann R, Brooks BP, Tamura D, Digiovanna JJ. Xeroderma pigmentosum, trichothiodystrophy and Cockayne syndrome: a complex genotype–phenotype relationship. *Neuroscience* 2007; **145**: 1388–1396.
2. Hayashi M. Role of oxidative stress in xeroderma pigmentosum. *Adv Exp Med Biol* 2008; **637**: 120–127.
3. Martin GM. Genetic modulation of senescent phenotypes in Homo sapiens. *Cell* 2005; **120**: 523–532.
4. Nance MA, Berry SA. Cockayne syndrome: review of 140 cases. *Am J Med Genet* 1992; **42**: 68–84.
5. Rapin I, Weidenheim K, Lindenbaum Y *et al.* Cockayne syndrome in adults: review with clinical and pathologic study of a new case. *J Child Neurol* 2006; **21**: 991–1006.
6. Shimoizumi H, Matsui M, Ito S, Miyao M, Kobayashi S. Cockayne syndrome complicated by acute subdural hemorrhage. *Brain Dev* 1995; **17**: 376.
7. Itoh M, Hayashi M, Shioda K *et al.* Neurodegeneration in hereditary nucleotide repair disorders. *Brain Dev* 1999; **21**: 326–333.
8. Cho WS, Batchuluun B, Lee SJ, Kang HS, Kim JE. Recurrent subdural hematoma from a pseudoaneurysm at the cortical branch of the middle artery after mild head injury: case report. *Neurol Med Chir (Tokyo)* 2011; **51**: 217–221.
9. Filippi S, Latini P, Frontini M, Palitti F, Egly JM, Proietti-De-Santis L. CSB protein is (a direct target of HIF-1 and) a critical mediator of the hypoxic response. *EMBO J* 2008; **27**: 2545–2556.
10. Brooks PJ, Cheng TF, Cooper L. Do all of the neurologic diseases in patients with DNA repair gene mutations result from the accumulation of DNA damage? *DNA Repair* 2008; **7**: 834–848.
11. Inoue T, Sano N, Ito Y *et al.* An adult case of Cockayne syndrome without sclerotic angiopathy. *Intern Med* 1997; **36**: 565–570.
12. Woody RC, Harding BN, Brumback RA, Leech RW. Absence of β-amyloid immunoreactivity in mesial temporal lobe in Cockyane's syndrome. *J Child Neurol* 1991; **6**: 32–34.
13. Mori H, Tomiyama T, Maeda N, Ozawa K, Wakasa K. Lack of amyloid plaque formation in the central nervous system of a patient with Werner syndrome. *Neuropathology* 2003; **23**: 51–56.

© 2011 Japanese Society of Neuropathology

14. van der Horst GT, Meira L, Gorgels TG *et al.* UVB radiation-induced cancer predisposition in Cockayne syndrome group A (Csa) mutant mice. *DNA Repair* 2002; **1**: 143–157.
15. van der Horst GT, van Steeg H, Berg RJ *et al.* Defective transcription-coupled repair in Cockayne syndrome B mice is associated with skin cancer predisposition. *Cell* 1997; **89**: 425–435.
16. Murai M, Enokido Y, Inamura N *et al.* Early postnatal ataxia and abnormal cerebellar development in mice lacking seroderma pigmentosum group A and Cockayne syndrome group B DNA repair genes. *Proc Natl Acad Sci U S A* 2001; **98**: 13379–13384.
17. Andressoo JO, Weeda G, de Wit J *et al.* An Xpb mouse model for combined xeroderma pigmentosum and Cockayne syndrome reveals progeroid features upon further attenuation of DNA repair. *Mol Cell Biol* 2009; **29**: 1276–1290.
18. *Neurodegenerative Diseases*, edited by Shamim I. Ahmad, from Landes Bioscience and Springer Science (ISBN: 978-1-4614-0652-5). http://www.landesbioscience.com/books/special/id/4242/
19. Mody N, Parhami F, Sarafian TA, Demer LL. Oxidative stress modulates osteoblastic differentiation of vascular and bone cells. *Free Radic Biol Med* 2001; **31**: 509–519.
20. Massy ZA, Maziere C, Kamel S *et al.* Impact of inflammation and oxidative stress on vascular calcifications in chronic kidney disease. *Pediatr Nephrol* 2005; **20**: 380–382.

© 2011 Japanese Society of Neuropathology

OPEN ACCESS Freely available online

PLoS one

Onset of Quiescence Following p53 Mediated Down-Regulation of H2AX in Normal Cells

Yuko Atsumi[1☯], Hiroaki Fujimori[1,3☯], Hirokazu Fukuda[2☯], Aki Inase[2], Keitaro Shinohe[3], Yoshiko Yoshioka[3], Mima Shikanai[3], Yosuke Ichijima[3], Junya Unno[4], Shuki Mizutani[4], Naoto Tsuchiya[2], Yoshitaka Hippo[2], Hitoshi Nakagama[2], Mitsuko Masutani[1], Hirobumi Teraoka[3], Ken-ichi Yoshioka[1,3]*

1 Division of Genome Stability Research, National Cancer Center Research Institute, Tokyo, Japan, **2** Division of Cancer Development System, National Cancer Center Research Institute, Tokyo, Japan, **3** Department of Pathological Biochemistry, Medical Research Institute, Tokyo Medical and Dental University, Tokyo, Japan, **4** Department of Pediatrics and Developmental Biology, Graduate School of Medical and Dental Sciences, Tokyo Medical and Dental University, Tokyo, Japan

Abstract

Normal cells, both *in vivo* and *in vitro*, become quiescent after serial cell proliferation. During this process, cells can develop immortality with genomic instability, although the mechanisms by which this is regulated are unclear. Here, we show that a growth-arrested cellular status is produced by the down-regulation of histone H2AX in normal cells. Normal mouse embryonic fibroblast cells preserve an H2AX diminished quiescent status through p53 regulation and stable-diploidy maintenance. However, such quiescence is abrogated under continuous growth stimulation, inducing DNA replication stress. Because DNA replication stress-associated lesions are cryptogenic and capable of mediating chromosome-bridge formation and cytokinesis failure, this results in tetraploidization. Arf/p53 module-mutation is induced during tetraploidization with the resulting H2AX recovery and immortality acquisition. Thus, although cellular homeostasis is preserved under quiescence with stable diploidy, tetraploidization induced under growth stimulation disrupts the homeostasis and triggers immortality acquisition.

Citation: Atsumi Y, Fujimori H, Fukuda H, Inase A, Shinohe K, et al. (2011) Onset of Quiescence Following p53 Mediated Down-Regulation of H2AX in Normal Cells. PLoS ONE 6(8): e23432. doi:10.1371/journal.pone.0023432

Editor: Michael Polymenis, Texas A&M University, United States of America

Received April 11, 2011; **Accepted** July 17, 2011; **Published** August 12, 2011

Copyright: © 2011 Atsumi et al. This is an open-access article distributed under the terms of the Creative Commons Attribution License, which permits unrestricted use, distribution, and reproduction in any medium, provided the original author and source are credited.

Funding: This study was supported by MEXT KAKENHI (20770136 and 20659047). The funders had no role in study design, data collection and analysis, decision to publish, or preparation of the manuscript.

Competing Interests: The authors have declared that no competing interests exist.

* E-mail: kyoshiok@ncc.go.jp

☯ These authors contributed equally to this work.

Introduction

Cancer is a disease associated with genomic instability and the accumulation of mutations [1]. Unlike specific chromosomal translocation-associated tumors, most cancers associated with aging develop either chromosomal instability (CIN) or microsatellite instability (MIN) [2]. While MIN is associated with mismatch repair deficiency, CIN develops even in a normal background [3]. However, the mechanisms by which CIN and MIN develop remain elusive.

A recent genomic analysis of various cancers revealed that massive genomic rearrangements, including loss of heterozygosity (LOH) and chromosomal translocation, amplification and deletion, do not gradually accumulate over time, as conventionally thought, but appear to be acquired in a single catastrophic event [4]. One of such events could be associated with tetraploidization because tetraploidy is a common early event in cancer cells with CIN [5]. Tetraploidy is observed in cells during the initial stages of cancer [6,7] as well as in precancerous stages such as dysplasia [8,9], but not in malignant cancer cells, which usually exhibit aneuploidy in association with deploidization [5]. Furthermore, analogous to changes observed in cancer genomes, the immortalization of mouse embryonic fibroblasts (MEFs) occurs with tetraploidy and mutation of the Arf/p53 module, which eventually evolves into aneuploidy during serial cultivation [10].

In the initial stages of carcinogenesis, cells are subjected to oncogenic stress, resulting in the accumulation of DNA replication stress-associated lesions and the onset of barrier responses such as senescence and apoptosis [11,12]. This effect can be reproduced *in vitro* by the activation of oncogenes [11] and accelerated growth stimulation [12] due to the induction of accelerated S-phase entry and the resulting DNA replication stress. Importantly, genomic instability is generated under these conditions [11,12] because DNA replication stress-associated lesions persist into M phase and mediate chromosomal bridge formation and cytokinesis failure, resulting in tetraploidization [10]. In fact, tetraploidization of MEFs is induced via chromosomal bridge formation prior to the onset of immortality with mutation of Arf/p53 [10], although it is still unclear how tetraploidization induces immortality. Since such tetraploidization is specifically observed during senescence, tetraploidization might be a defect that occurs during cell proliferation or growth arrest. In fact, similar to cells in the initial stages of carcinogenesis, senescent cells often accumulate irreparable DNA lesions [13,14] and frequently exhibit genomic instability [15].

The development of cancer, as well as the onset of immortality in cells *in vitro*, is tightly associated with mutations in the Arf/p53 module [16–18]. Although this is ascribed to the role of p53 in

cancer prevention, the regulation and roles of p53 are complex [18]. While constitutively active p53 mediates premature aging in mice [19–21], additional single gene copies of *Arf* and *p53* under functional regulation mediate longevity and cancer prevention [22]. Similarly, while the accumulation of p53 induces cellular senescence and apoptosis [16,17], additional single gene copies of *Arf* and *p53* in MEFs has a protective effect from immortalization [22], suggesting that they help to maintain homeostasis under undamaged conditions. This raises the questions of the identity of the regulatory target of p53 in preserving cellular homeostasis under normal conditions and how cellular homeostasis preservation and abrogation are associated with genomic status and p53 regulation.

This study focused on the mechanism by which normal cells under serial proliferation regulate homeostasis preservation and abrogation and sought to identify the regulatory target of p53. Our results illustrated two distinct conditions that could result in growth-arrested cells: (i) cells that maintain continuous quiescence by down-regulating H2AX (a variant of core histone H2A) under p53 regulation and stable-diploidy maintenance; and (ii) cells that develop tetraploidy and immortality under continuous growth stimulation, characterized by the accumulation of γH2AX foci. Thus, oncogenic stress under growth stimulation triggers catastrophic tetraploidization that leads to immortalization in association with the accompanying mutation of the Arf/p53 module and recovery of H2AX expression and growth activity.

Results

Immortality is prevented in quiescent cells that maintain genomic stability

MEFs cultured under the standard 3T3 protocol (Std-3T3) senesce in association with oxygen sensitivity [23], which is followed by the development of immortality with tetraploidy [10] and mutation of the Arf/p53 module [22], similar to the process of carcinogenesis. In addition, similar to cells in the initial stages of carcinogenesis, spontaneous DNA lesions accumulate in senescent MEFs under Std-3T3 conditions prior to the development of immortality [10], which suggests that growth stimulation induced under Std-3T3 conditions might overwhelm senescent MEFs. Therefore, MEFs under Std-3T3 conditions were compared with MEFs exposed to temporary serum deprivation (tSD-3T3), which induces occasional growth arrest (Fig. 1A). Under Std-3T3 conditions, MEFs were immortalized with tetraploidy that progresses to aneuploidy (Fig. 1A–C). On the other hand, MEFs cultured under tSD-3T3 conditions never developed immortality and preserved quiescence with stable diploidy (Fig. 1A, C). This indicates that temporal growth arrest prevents immortalization and supports genomic stability. Conversely, continuous culture with 10% FBS produces oncogenic stress in senescent MEFs, triggering tetraploidization. Thus, even though both are growth arrested (at least in total cell numbers) with senescent morphology at the same culture passage (P9) (Fig. S1), MEFs under tSD-3T3 conditions are continuously quiescent with genomic stability, while MEFs under Std-3T3 conditions develop tetraploidy (Fig. 1A, C), posing a question in DNA lesion status that induces chromosomal bridge formation and tetraploidization [10].

γH2AX foci accumulate in cells developing genomic instability but not in cells preserving diploidy

To determine the DNA lesion status induced by accelerated growth stimulation, γH2AX foci were compared in growth-arrested MEFs (P9) under both conditions (Fig. 1D). As expected, MEFs that developed tetraploidy under Std-3T3 conditions accumulated γH2AX foci, with some carrying over into the G2/M phases (Fig. 1E). This resulted in chromosome bridge formation (Fig. 1F) with the resulting tetraploidization that is initially observed with binucleated tetraploidy (Fig. 1F). On the other hand, quiescent MEFs that preserved genomic stability under tSD-3T3 conditions did not develop γH2AX foci (Fig. 1D), indicating that genomic stability is preserved under no γH2AX signal. However, it was still unclear why quiescent MEFs under tSD-3T3 conditions do not accumulate γH2AX foci because senescent cells are known to generally accumulate irreparable DNA lesions [13,14].

To address why γH2AX foci do not form under tSD-3T3 conditions, the expression level of H2AX at P9 was determined. As shown in Figure 1G, a remarkable reduction in H2AX expression was observed in quiescent MEFs at P9 while MEFs that developed tetraploidy under Std-3T3 conditions showed significantly higher H2AX expression than quiescent MEFs. This illustrates an association between H2AX levels and the cellular and genomic status, in that cells with largely diminished H2AX expression preserve stable diploidy and a quiescent status, while cells with residual H2AX expression and with γH2AX foci develop genomic instability and immortality (Fig. 1H). Importantly, H2AX-KO cells exhibited impaired DNA repair, growth retardation, and elevated genomic instability [24–28], phenotypes reminiscent of senescent cells. Therefore, it will be critical to determine how H2AX-status is regulated to produce quiescence and induce genomic instability.

H2AX is generally diminished in quiescent cells

To address whether H2AX diminution is a general occurrence, H2AX expression was compared in normal human fibroblasts (NHFs) and MEFs. Decreased H2AX was observed in both cell types at growth-arrested stage after serial proliferation (Fig. 2A, B), suggesting that this process is conserved between humans and mice. In addition, H2AX diminution was also observed in many organs of adult mice, including the liver, spleen, and pancreas (Fig. 2C, D; Fig. S2). Thus, H2AX is generally reduced in quiescent cell chromosomes both *in vitro* and *in vivo*.

H2AX is also diminished during premature senescence induced by DNA damage. Using early passage MEFs (P2), H2AX diminution was observed when senescence was induced by treatment with hydroxyurea (HU) to induce DNA replication stress (Fig. 2E) and with the radiomimetic DNA-damaging agent, neocarzinostatin (Fig. S3). This most likely occurs because DNA repair is coupled with H2AX release and chromatin remodeling [29–31]. Together with results showing a decrease in H2AX transcript levels in senescent MEFs (Fig. S4), these results indicate that decreased amounts of H2AX protein in senescing cells is ascribed to a decrease in H2AX transcript levels and DNA damage.

To directly address the impact of H2AX reduction, H2AX was knocked down in early passage NHFs, which induced cellular quiescence with senescent cell characteristics; cells adopted a flattened and enlarged morphology and showed an increase in senescence-associated β-galactosidase activity (Fig. 2F). Since the knockdown of H2AX in 293T cells induced growth arrest without inducing a senescent morphology (data not shown), it is likely that the effect of H2AX diminution is primarily due to quiescence induction and potentially a normal consequence of senescence in normal cells.

Immortalized cells develop following tetraploidization when H2AX status and growth activity are restored

The above results illustrate that cellular quiescence is produced when cells maintain stable diploidy and diminished H2AX

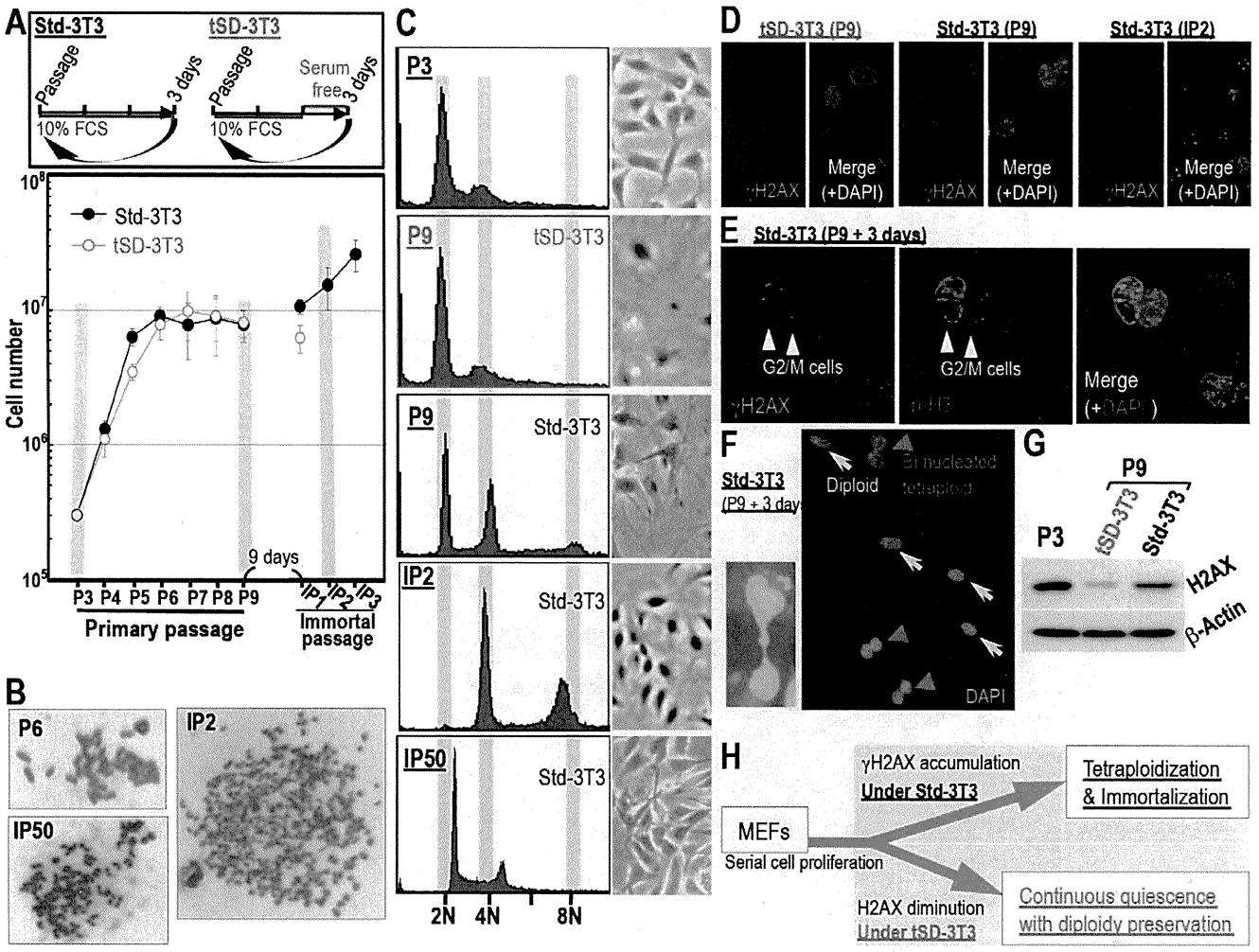

Figure 1. Immortality with tetraploidy is blocked in quiescent cells with diploidy, diminished H2AX, and no γH2AX foci. A. Growth curves of MEFs cultured under the standard 3T3 protocol (Std-3T3) or the T3 protocol with temporary serum deprivation (tSD-3T3) as schematically shown. MEFs under Std-3T3 conditions were immortalized, whereas MEFs cultured under tSD-3T3 conditions were not. **B** Genomic instability developed in immortalized MEFs (IP2) under Std-3T3 conditions. **C.** Genomic status was determined by flow-cytometry at the indicated conditions and passages. Representative images are shown. Tetraploidy development was blocked under tSD-3T3 conditions, while tetraploidy had already developed in growth-arrested MEFs at P9 under Std-3T3 conditions (see increasing 4N and 8N peaks). **D.** DNA lesions identified by γH2AX foci spontaneously accumulated in MEFs developing tetraploidy and immortality (P9) under Std-3T3 conditions as well as in immortal cells (IP2), while MEFs that maintained quiescent status with genomic stability under tSD-3T3 conditions contained no foci. **E.** DNA lesion-carryover into the G2-M phases was determined for lesions that spontaneously accumulated in senescent MEFs under Std-3T3 conditions. DNA lesions in senescing MEFs are also observed in the G2-M phases determined by phosphorylated H3. **F.** Chromosome bridge formation (Left panel) is observed in association with DNA lesion-carryover into the G2-M phases under Std-3T3 conditions with the resulting accumulation of bi-nucleated tetraploidy (Right panel: red arrow heads). Representative images are shown. **G.** The total H2AX level at P9 under each condition was determined. Whereas a significant reduction in H2AX expression was observed in MEFs with genomic stability under tSD-3T3 conditions, MEFs that developed immortality and genomic instability under Std-3T3 conditions did not show a significant decrease in H2AX expression. **H.** A model of the life-cycle of MEFs undergoing quiescence or developing immortality. While quiescent MEFs preserve diploidy and show diminished H2AX levels, MEFs developing immortality exhibited γH2AX foci accumulation.

doi:10.1371/journal.pone.0023432.g001

expression. In these cells, the H2AX level is less than 100-fold compared to that in actively growing cells. To study the effect of growth stimulation in cells with an H2AX-diminished quiescent status, complete medium (DMEM with 10% FBS) was added to quiescent MEFs prepared under tSD-3T3 conditions (Fig. 3A–C). In these cells, cell-cycle progression was initiated with the expression of PCNA and histones H3 and H2AX, which led to γH2AX foci formation (Fig. 3D, E). Abrogating quiescent status with complete medium resulted in the establishment of immortalized MEFs with tetraploidy (Fig. 3A–C). However, it took 30 days to initiate immortal passage in H2AX-diminished quiescent MEFs, while immortality was acquired in only 9 days for P9 MEFs under Std-3T3 conditions, suggesting that the H2AX-diminished quiescent status protected cells from immortalization. Supporting this argument, primary MEFs transfected with an H2AX expression vector also acquired immortality at an accelerated rate (Fig. S5A–C). Such H2AX-overexpression may induce the effect of DNA replication stress because immortality in H2AX-overexpressing MEFs were again developed with tetraploidy (Fig. S5D,E). Unexpectedly, H2AX status was totally recovered in actively growing, immortalized MEFs (Fig. 3F, G), which illustrates the association of H2AX status with growth activity.

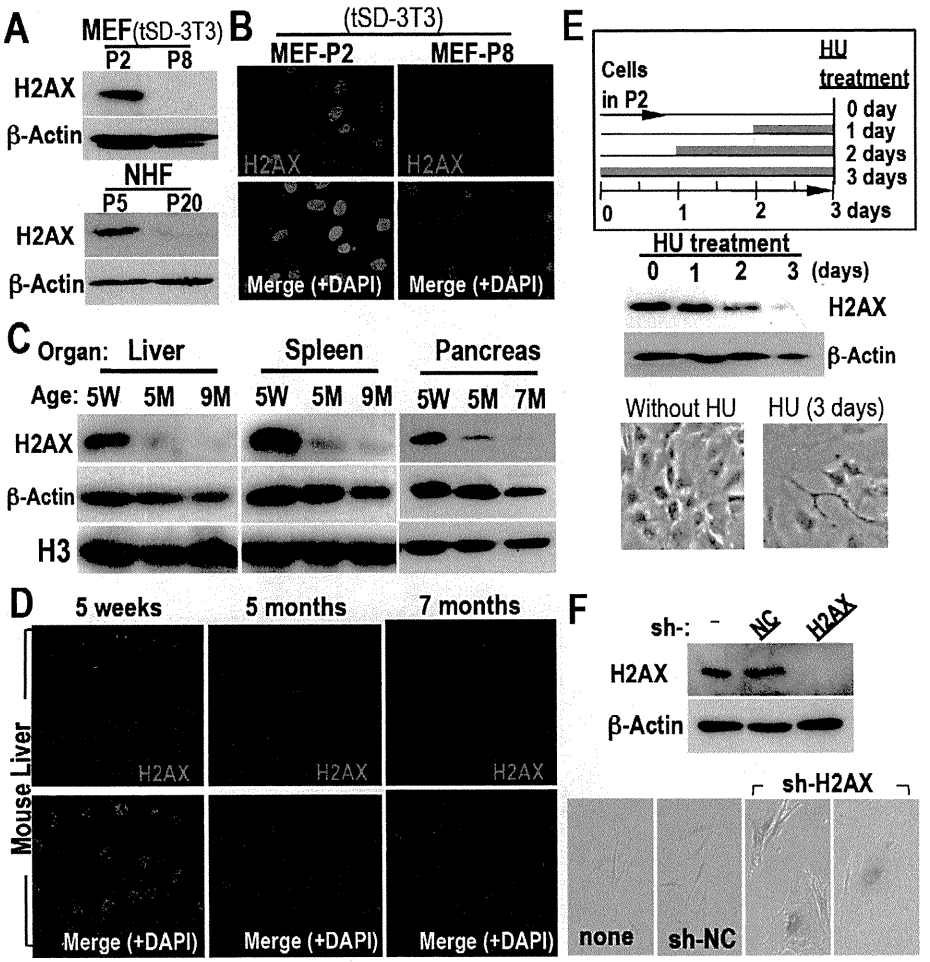

Figure 2. Quiescent cell-status is induced with H2AX diminution both *in vitro* and *in vivo*. A,B H2AX expression in growth-arrested cells (P8 for MEFs under tSD-3T3 conditions, P20 for NHFs) was determined by Western blotting (**A**) and immunofluorescent staining (**B**), revealing H2AX diminution in both types of growth-arrested cells. **C,D** H2AX diminution was also measured in adult mice organs by Western blotting (**C**) and in liver sections by immunofluorescent staining (**D**). Samples were prepared from five week (5W), five month (5M) and seven- or nine-month-old mice (7M or 9M). **E.** The involvement of H2AX diminution in DNA damage-induced premature senescence was determined after 0.2 mM HU treatment. Orange bars indicate the periods of HU treatment. Premature damage-induced senescence was observed with H2AX diminution, in which cells were flattened and enlarged, morphology typical of senescent cells. **F.** The effect of H2AX knockdown on senescence was determined in NHFs. Senescence was directly induced by H2AX knockdown in NHFs. H2AX status and senescence was determined by Western blotting (top) and SA-β-gal activation, and cells exhibited a flattened and enlarged morphology (bottoms), respectively.
doi:10.1371/journal.pone.0023432.g002

However, this also poses the question of how the down-regulation of H2AX expression in quiescent MEFs is reversed after immortalization.

Immortalized cells no longer achieve H2AX diminution-associated quiescent status

To explore the effects of the change in H2AX status, the response of H2AX to DNA replication stress was compared between primary and immortalized MEFs. While H2AX in primary MEFs was down-regulated after HU treatment, this did not occur in immortalized MEFs (Fig. 3H), which indicates that H2AX diminution-associated quiescent cell status is not inducible after immortalization. Thus, quiescent status is preserved in cells with diminished H2AX expression and stable diploidy but is abrogated under continuous growth stimulation, inducing cell cycle progression and γH2AX foci formation, and eventually leading to immortality with tetraploidy and H2AX recovery. Since the Arf/p53 module is specifically mutated during MEF immortalization [22], p53 might be involved in H2AX down-regulation. In fact, unlike senescent normal cells, H2AX expression is relatively high (2–20% of total H2A) in cancer cells as well as in growing NHFs (10%) [28].

H2AX diminution-associated quiescent status is produced by p53 and prohibits the development of immortality

To determine the involvement of p53 in H2AX down-regulation, *p53* knockout (KO) MEFs were cultured. Unlike normal primary MEFs, but similar to immortalized MEFs (Fig. 3H), H2AX expression in primary *p53*-KO-MEFs was not decreased by HU treatment (Fig. 4A). Furthermore, *p53*-KO-MEFs continuously grew, without change in H2AX status even under tSD-3T3 conditions (Fig. 4B, C). This indicates that H2AX in wild-type (WT)-MEFs is down-regulated by p53 to

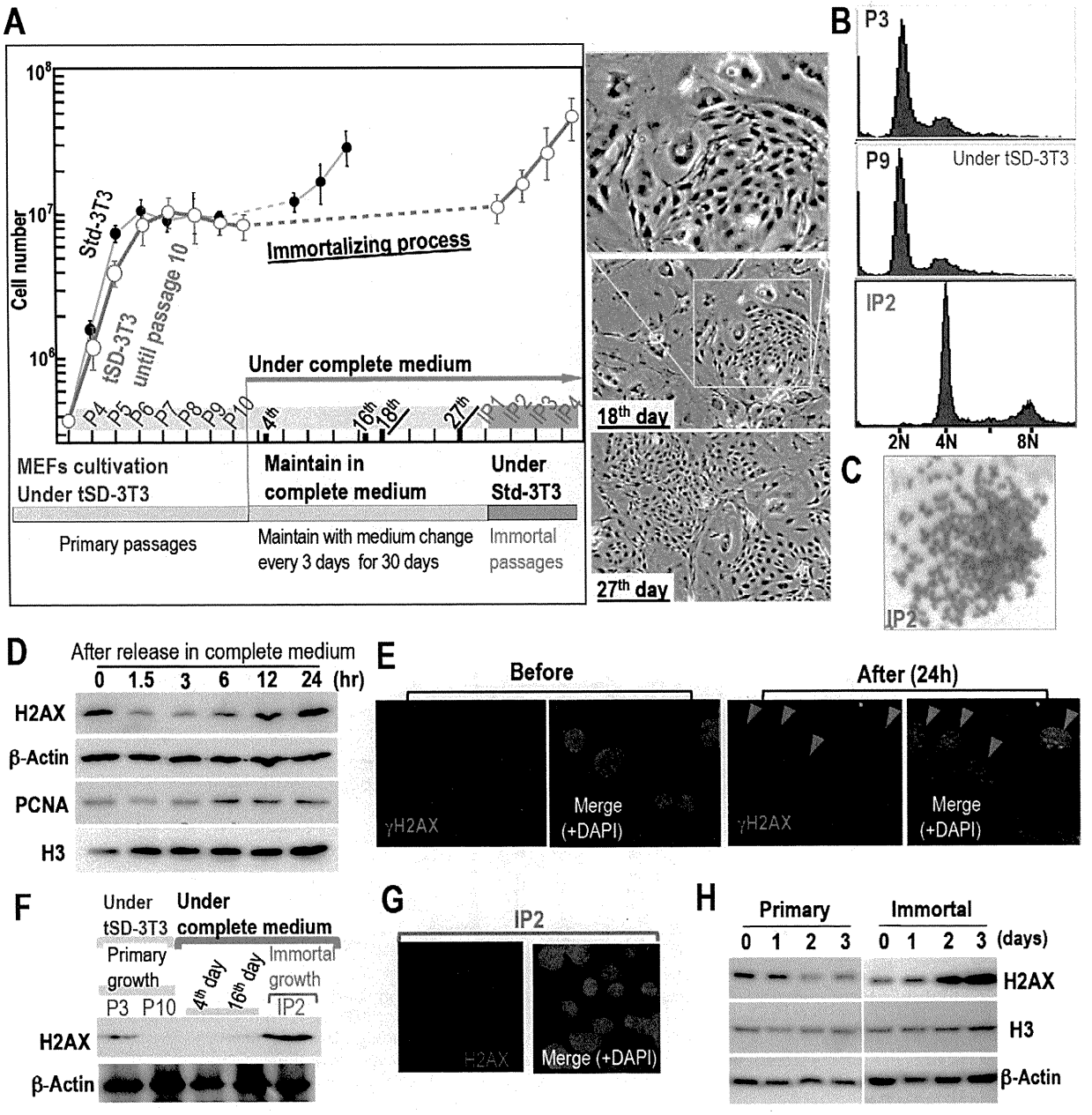

Figure 3. H2AX-diminished quiescent cell-status is abolished by continuous growth stimulation with accompanying H2AX recovery. A. Quiescent MEFs with diminished H2AX expression were cultured under tSD-3T3 conditions until P10. They were then exposed to complete medium, which was changed every three days for 30 days. Immortal passages were started under Std-3T3 conditions (red circles). MEFs cultured under the Std-3T3 conditions (black circles) as in Figure 1a were superimposed for comparison of the time needed to acquire immortality. Representative images of MEFs during the process of acquiring immortality are also shown. **B,C.** Tetraploidy development in immortalized MEFs (IP2) was observed by flow-cytometry (**B**) and Giemsa staining (**C**). **D.** Growth acceleration-associated cell cycle progression and H2AX induction. To determine the effect of serum induction on H2AX expression and cell cycle progression, senescent MEFs at P8 were incubated in serum-free medium for 24 h and harvested after exposure to complete medium for various times. H2AX expression increased with increasing PCNA and histone H3, which suggests that the expression of these chromatin factors was associated with S phase entry. To detect H2AX levels in these MEFs at P8, the H2AX signal was visualized by longer exposure. **E.** DNA lesions characterized by γH2AX foci were induced in MEFs (red arrowheads) after exposure to complete medium as in **D**. **F,G.** H2AX status in immortalized MEFs was determined by Western blotting (**F**) and immunofluorescence (**G**), revealing H2AX recovery. **H.** DNA replication stress-associated H2AX diminution was compared between normal and immortalized MEFs as in Figure 2E, in which H2AX was not down-regulated after immortalization.
doi:10.1371/journal.pone.0023432.g003

induce cellular quiescence and is recovered in immortalized MEFs in association with tetraploidization and mutation of the Arf/p53 module. Although *p53*-KO-MEFs did not undergo H2AX diminution-mediated growth arrest, these MEFs still exhibited a senescent morphology (Fig. 4D, see P8) and subsequently achieved an immortalized morphology (P14), which suggests the immortalization of *p53*-KO-MEFs via the senescent stage without growth arrest. This also indicates that a quiescent cell status is induced by p53 to protect cells from immortality.